

# Full-Duplex MIMO Relaying: Achievable Rates under Limited Dynamic Range

Brian P. Day,<sup>\*</sup> Adam R. Margetts,<sup>†</sup> Daniel W. Bliss,<sup>†</sup> and Philip Schniter<sup>\*‡</sup>

**Abstract**—In this paper we consider the problem of full-duplex multiple-input multiple-output (MIMO) relaying between multi-antenna source and destination nodes. The principal difficulty in implementing such a system is that, due to the limited attenuation between the relay's transmit and receive antenna arrays, the relay's outgoing signal may overwhelm its limited-dynamic-range input circuitry, making it difficult—if not impossible—to recover the desired incoming signal. While explicitly modeling transmitter/receiver dynamic-range limitations and channel estimation error, we derive tight upper and lower bounds on the end-to-end achievable rate of decode-and-forward-based full-duplex MIMO relay systems, and propose a transmission scheme based on maximization of the lower bound. The maximization requires us to (numerically) solve a nonconvex optimization problem, for which we detail a novel approach based on bisection search and gradient projection. To gain insights into system design tradeoffs, we also derive an analytic approximation to the achievable rate and numerically demonstrate its accuracy. We then study the behavior of the achievable rate as a function of signal-to-noise ratio, interference-to-noise ratio, transmitter/receiver dynamic range, number of antennas, and training length, using optimized half-duplex signaling as a baseline.

**Keywords:** MIMO relays, full-duplex relays, limited dynamic range, channel estimation.

## I. INTRODUCTION

We consider the problem of communicating from a source node to a destination node through a relay node. Traditional relay systems operate in a half-duplex mode, whereby the time-frequency signal-space used for the source-to-relay link is kept orthogonal to that used for the relay-to-destination link, such as with non-overlapping time periods or frequency bands. Half-duplex operation is used to avoid the high levels of relay self-interference that are faced with full-duplex<sup>1</sup> operation (see Fig. 1), where the source and relay share a common time-frequency signal-space. For example, it is not unusual for the ratio between the relay's self-interference power and desired

incoming signal power to exceed 100 dB [3], or—in general—some value larger than the dynamic range of the relay's front-end hardware, making it impossible to recover the desired signal. The importance of *limited dynamic-range* (DR) cannot be overstressed; notice that, even if the self-interference signal was perfectly known, limited-DR renders perfect cancellation impossible.

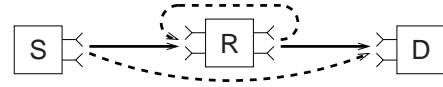


Fig. 1. Full-duplex MIMO relaying from source to destination. Solid lines denote desired propagation and dashed lines denote interference.

Recently, multiple-input multiple-output (MIMO) relaying has been proposed as a means of increasing spectral efficiency (e.g., [4], [5]). By MIMO relaying, we mean that the source, relay, and destination each use multiple antennas for both reception and transmission. MIMO relaying brings the possibility of full-duplex operation through *spatial* self-interference suppression (e.g., [3], [6]–[15]). As a simple example, one can imagine using the relay's transmit array to form spatial nulls at a subset of the relay's receive antennas, which are then free of self-interference and able to recover the desired signal. In forming these nulls, however, it can be seen that the relay consumes spatial degrees-of-freedom that could have been used in communicating data to the destination. Thus, maximizing the end-to-end throughput involves navigating a tradeoff between the source-to-relay link and relay-to-destination link. Of course, maximizing end-to-end throughput is more involved than simply protecting an arbitrary subset of the relay's receive antennas; one also needs to consider which subset to protect, and the degree to which each of those antennas are protected, given the source-to-relay and relay-to-destination MIMO channel coefficients, the estimation errors on those coefficients, and the DR limitations of the various nodes. These considerations motivate the following fundamental questions about full-duplex MIMO relaying in the presence of self-interference: 1) *What is the maximum achievable end-to-end throughput under a transmit power constraint?* 2) *How can the system be designed to achieve this throughput?*

In this paper, we aim to answer these two fundamental questions while paying special attention to the effects of both limited-DR and channel estimation error.

- 1) Limited-DR is a natural consequence of non-ideal amplifiers, oscillators, analog-to-digital converters (ADCs), and digital-to-analog converters (DACs). To model the

<sup>\*</sup>Brian Day and Philip Schniter are with the Department of Electrical and Computer Engineering, The Ohio State University, Columbus, OH.

<sup>†</sup>Daniel Bliss and Adam Margetts are with the Advanced Sensor Techniques Group, MIT Lincoln Laboratory, Lexington, MA.

<sup>‡</sup>Please direct all correspondence to Prof. Philip Schniter, Dept. ECE, The Ohio State University, 2015 Neil Ave., Columbus OH 43210, e-mail: schniter@ece.osu.edu, phone 614.247.6488, fax 614.292.7596.

Manuscript received August 25, 2011; revised May 14, 2012.

This work was sponsored by the Defense Advanced Research Projects Agency under Air Force contract FA8721-05-C-0002. Opinions, interpretations, conclusions, and recommendations are those of the authors and are not necessarily endorsed by the United States Government.

<sup>1</sup>Successful full-duplex communication has been recently demonstrated in the non-relay setting [1] and in the non-MIMO relay setting [2].

effects of limited receiver-DR, we inject, at each receive antenna, an additive white Gaussian “receiver distortion” with variance  $\beta$  times the energy impinging on that receive antenna (where  $\beta \ll 1$ ). Similarly, to model the effects of limited transmitter-DR, we inject, at each transmit antenna, an additive white Gaussian “transmitter noise” with variance  $\kappa$  times the energy of the intended transmit signal (where  $\kappa \ll 1$ ). Thus,  $\kappa^{-1}$  and  $\beta^{-1}$  characterize the transmitter and receiver dynamic ranges, respectively.

- 2) Imperfect CSI can result for several reasons, including channel time-variation, additive noise, and DR limitations. We focus on CSI imperfections that result from the use of pilot-aided least-squares (LS) channel estimation performed in the presence of limited-DR.

Moreover, we consider regenerative relays that decode-and-forward (as in [3], [6]–[10]), as opposed to simpler non-regenerative relays that only amplify-and-forward (as in [11]–[15]).

The contributions of this paper are as follows. For the full-duplex MIMO relaying problem, an explicit model for transmitter/receiver-DR limitations is proposed; pilot-aided least-squares MIMO-channel estimation, under DR limitations, is analyzed; the residual self-interference, from DR limitations and channel-estimation error, is analyzed; lower and upper bounds on the achievable rate are derived; a transmission scheme is proposed based on maximizing the achievable-rate lower bound subject to a power constraint, requiring the solution of a nonconvex optimization problem, to which we apply bisection search and Gradient Projection; an analytic approximation of the maximum achievable rate is proposed; and, the achievable rate is numerically investigated as a function of signal-to-noise ratio, interference-to-noise ratio, transmitter/receiver dynamic range, number of antennas, and number of pilots.

The paper is structured as follows. In Section II, we state our channel model, limited-DR model, and assumptions on the transmission protocol. Then, in Section III, we derive upper and lower bounds on the achievable rate under pilot-aided channel estimation and partial self-interference cancellation at the relay. In Section IV, we propose a novel transmission scheme that is based on maximizing the achievable-rate lower-bound subject to a power constraint and, in Section V, we derive a closed-form approximation of the optimized achievable rate whose accuracy is numerically verified. Then, in Section VI, we numerically investigate achievable rate as a function of the SNRs ( $\rho_r, \rho_d$ ), the INRs ( $\eta_r, \eta_d$ ), the dynamic range parameters ( $\kappa, \beta$ ), the number of antennas ( $N_r, N_d$ ), and the training length  $T$ , and we also investigate the gain of full-duplex signaling (over half-duplex) and partial self-interference cancellation. Finally, in Section VII, we conclude.

*Notation:* We use  $(\cdot)^T$  to denote transpose,  $(\cdot)^*$  conjugate, and  $(\cdot)^H$  conjugate transpose. For matrices  $\mathbf{A}, \mathbf{B} \in \mathbb{C}^{M \times N}$ , we use  $\text{tr}(\mathbf{A})$  to denote trace,  $\det(\mathbf{A})$  to denote determinant,  $\mathbf{A} \odot \mathbf{B}$  to denote elementwise (i.e., Hadamard) product,  $\text{sum}(\mathbf{A}) \in \mathbb{C}$  to denote the sum over all elements,  $\text{vec}(\mathbf{A}) \in \mathbb{C}^{MN}$  to denote vectorization,  $\text{diag}(\mathbf{A})$  to denote the diagonal matrix with the same diagonal elements as  $\mathbf{A}$ ,  $\text{Diag}(\mathbf{a})$  to denote the

diagonal matrix whose diagonal is constructed from the vector  $\mathbf{a}$ , and  $[\mathbf{A}]_{m,n}$  to denote the element in the  $m^{\text{th}}$  row and  $n^{\text{th}}$  column of  $\mathbf{A}$ . We denote expectation by  $\mathbb{E}\{\cdot\}$ , covariance by  $\text{Cov}\{\cdot\}$ , statistical independence by  $\perp$ , the circular complex Gaussian pdf with mean vector  $\mathbf{m}$  and covariance matrix  $\mathbf{Q}$  by  $\mathcal{CN}(\mathbf{m}, \mathbf{Q})$ , and the Kronecker delta sequence by  $\delta_k$ . Finally,  $\mathbf{I}$  denotes the identity matrix,  $\mathbb{C}$  the complex field, and  $\mathbb{Z}^+$  the positive integers.

## II. SYSTEM MODEL

We will use  $N_s$  and  $N_r$  to denote the number of transmit antennas at the source and relay, respectively, and  $M_r$  and  $M_d$  to denote the number of receive antennas at the relay and destination, respectively. Here and in the sequel, we use subscript-s for source, subscript-r for relay, and subscript-d for destination. Similarly, we will use subscript-sr for source-to-relay, subscript-rd for relay-to-destination, subscript-rr for relay-to-relay, and subscript-sd for source-to-destination. At times, we will omit the subscripts when referring to common quantities. For example, we will use  $\mathbf{s}(t) \in \mathbb{C}^N$  to denote the time  $t \in \mathbb{Z}^+$  noisy signals radiated by the transmit antenna arrays, and  $\mathbf{u}(t) \in \mathbb{C}^M$  to denote the time- $t$  undistorted signals collected by the receive antenna arrays. More specifically, the source’s and relay’s radiated signals are  $\mathbf{s}_s(t) \in \mathbb{C}^{N_s}$  and  $\mathbf{s}_r(t) \in \mathbb{C}^{N_r}$ , respectively, while the relay’s and destination’s collected signals are  $\mathbf{u}_r(t) \in \mathbb{C}^{M_r}$  and  $\mathbf{u}_d(t) \in \mathbb{C}^{M_d}$ , respectively.

### A. Propagation Channels

We assume that propagation between each transmitter-receiver pair can be characterized by a Rayleigh-fading MIMO channel  $\mathbf{H} \in \mathbb{C}^{M \times N}$  corrupted by additive white Gaussian noise (AWGN)  $\mathbf{n}(t)$ . By “Rayleigh fading,” we mean that  $\text{vec}(\mathbf{H}) \sim \mathcal{CN}(\mathbf{0}, \mathbf{I}_{MN})$ , and by “AWGN,” we mean that  $\mathbf{n}(t) \sim \mathcal{CN}(\mathbf{0}, \mathbf{I}_M)$ . The time- $t$  radiated signals  $\mathbf{s}(t)$  are then related to the received signals  $\mathbf{u}(t)$  via

$$\mathbf{u}_r(t) = \sqrt{\rho_r} \mathbf{H}_{sr} \mathbf{s}_s(t) + \sqrt{\eta_r} \mathbf{H}_{rr} \mathbf{s}_r(t) + \mathbf{n}_r(t) \quad (1)$$

$$\mathbf{u}_d(t) = \sqrt{\rho_d} \mathbf{H}_{rd} \mathbf{s}_r(t) + \sqrt{\eta_d} \mathbf{H}_{sd} \mathbf{s}_s(t) + \mathbf{n}_d(t). \quad (2)$$

In (1)-(2),  $\rho_r > 0$  and  $\rho_d > 0$  denote the signal-to-noise ratio (SNR) at the relay and destination, while  $\eta_r > 0$  and  $\eta_d > 0$  denote the interference-to-noise ratio (INR) at the relay and destination. (As described in the sequel, the destination treats the source-to-destination link as interference). The INR  $\eta_r$  will depend on the separation between, and orientation of, the relay’s transmit and receive antenna arrays [10], whereas the INR  $\eta_d$  will depend on the separation between source and destination modems, so that typically  $\eta_d \ll \eta_r$ . We emphasize that (1)-(2) models the channels  $\mathbf{H}_{sr}$ ,  $\mathbf{H}_{rr}$ ,  $\mathbf{H}_{rd}$ , and  $\mathbf{H}_{sd}$ , as time-invariant quantities.

### B. Transmission Protocol

For full-duplex decode-and-forward relaying, we partition the time indices  $t = 0, 1, 2, \dots$  into a sequence of communication epochs  $\{\mathcal{T}_i\}_{i=0}^\infty$  where, during epoch  $\mathcal{T}_i \subset \mathbb{Z}^+$ , the source communicates the  $i^{\text{th}}$  information packet to the relay,

while simultaneously the relay communicates the  $(i-1)^{th}$  information packet to the destination. Before the first data communication epoch, we assume the existence of a training epoch  $\mathcal{T}_{\text{train}}$  during which the modems estimate the channel state. From the estimated channel state, the data communication design parameters are optimized and the resulting parameters are used for every data communication epoch. Since the design and analysis will be identical for every data-communication epoch (as a consequence of channel time-invariance), we suppress the index  $i$  in the sequel and refer to an arbitrary data communication epoch as  $\mathcal{T}_{\text{data}}$ .

The training epoch is partitioned into two equal-length periods (i.e.,  $\mathcal{T}_{\text{train}}[1]$  and  $\mathcal{T}_{\text{train}}[2]$ ) to avoid self-interference when estimating the channel matrices. Each data epoch is also partitioned into two periods (i.e.,  $\mathcal{T}_{\text{data}}[1]$  and  $\mathcal{T}_{\text{data}}[2]$ ) of normalized duration  $\tau \in [0, 1]$  and  $1 - \tau$ , respectively, over which the transmission parameters can be independently optimized. As we shall see in the sequel, such flexibility is critical when the INR  $\eta_r$  is large relative to the SNR  $\rho_r$ . Moreover, this latter partitioning allows us to formulate both half- and full-duplex schemes as special cases of a more general transmission protocol. For use in the sequel, we find it convenient to define  $\tau[1] \triangleq \tau$  and  $\tau[2] \triangleq 1 - \tau$ . Within each of these periods, we assume that the transmitted signals are zero-mean and wide-sense stationary.

### C. Limited Transmitter Dynamic Range

We model the effect of limited transmitter dynamic range (DR) by injecting, per transmit antenna, an independent zero-mean Gaussian “transmitter noise” whose variance is  $\kappa$  times the energy of the *intended* transmit signal at that antenna. In particular, say that  $\mathbf{x}(t) \in \mathbb{C}^N$  denotes the transmitter’s intended time- $t$  transmit signal, and say  $\mathbf{Q} \triangleq \text{Cov}\{\mathbf{x}(t)\}$  over the relevant time period (e.g.,  $t \in \mathcal{T}_{\text{data}}[1]$ ). We then write the time- $t$  noisy radiated signal as

$$\mathbf{s}(t) = \mathbf{x}(t) + \mathbf{c}(t) \text{ s.t. } \begin{cases} \mathbf{c}(t) \sim \mathcal{CN}(\mathbf{0}, \kappa \text{diag}(\mathbf{Q})) \\ \mathbf{c}(t) \perp\!\!\!\perp \mathbf{x}(t) \\ \mathbf{c}(t) \perp\!\!\!\perp \mathbf{c}(t')|_{t' \neq t} \end{cases}, \quad (3)$$

where  $\mathbf{c}(t) \in \mathbb{C}^N$  denotes transmitter noise and  $\perp\!\!\!\perp$  statistical independence. Typically,  $\kappa \ll 1$ . As shown by measurements of various hardware setups (e.g., [16], [17]), the independent Gaussian noise model in (3) closely approximates the combined effects of additive power-amp noise, non-linearities in the DAC and power-amp, and oscillator phase noise. Moreover, the dependence of the transmitter-noise variance on intended signal power in (3) follows directly from the definition of limited dynamic range.

### D. Limited Receiver Dynamic Range

We model the effect of limited receiver-DR by injecting, per receive antenna, an independent zero-mean Gaussian “receiver distortion” whose variance is  $\beta$  times the energy collected by that antenna. In particular, say that  $\mathbf{u}(t) \in \mathbb{C}^M$  denotes the receiver’s undistorted time- $t$  received vector, and say  $\Phi \triangleq$

$\text{Cov}\{\mathbf{u}(t)\}$  over the relevant time period (e.g.,  $t \in \mathcal{T}_{\text{data}}[1]$ ). We then write the distorted post-ADC received signal as

$$\mathbf{y}(t) = \mathbf{u}(t) + \mathbf{e}(t) \text{ s.t. } \begin{cases} \mathbf{e}(t) \sim \mathcal{CN}(\mathbf{0}, \beta \text{diag}(\Phi)) \\ \mathbf{e}(t) \perp\!\!\!\perp \mathbf{u}(t) \\ \mathbf{e}(t) \perp\!\!\!\perp \mathbf{e}(t')|_{t' \neq t} \end{cases}, \quad (4)$$

where  $\mathbf{e}(t) \in \mathbb{C}^M$  is additive distortion. Typically,  $\beta \ll 1$ . From a theoretical perspective, automatic gain control (AGC) followed by dithered uniform quantization [18] yields quantization errors whose statistics closely match the model (4). More importantly, studies (e.g., [19]) have shown that the independent Gaussian distortion model (4) accurately captures the combined effects of additive AGC noise, non-linearities in the ADC and gain-control, and oscillator phase noise in practical hardware.

Figure 2 summarizes our model. The dashed lines indicate that the distortion levels are proportional to mean energy levels and not to the instantaneous value.

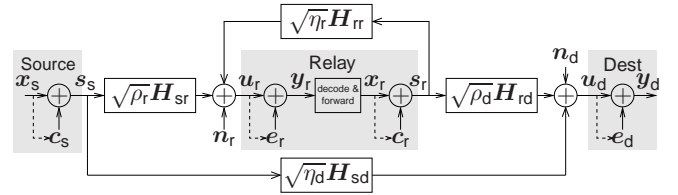


Fig. 2. Our model of full-duplex MIMO relaying under limited transmitter/receiver-DR. The dashed lines denote statistical dependence.

## III. ANALYSIS OF ACHIEVABLE RATE

### A. Pilot-Aided Channel Estimation

In this section, we describe the pilot-aided channel estimation procedure that is used to learn the channel matrices  $\mathbf{H}$ . In our protocol, the training epoch consists of two periods,  $\mathcal{T}_{\text{train}}[1]$  and  $\mathcal{T}_{\text{train}}[2]$ , each spanning  $TN$  channel uses (for some  $T \in \mathbb{Z}^+$ ). For all times  $t \in \mathcal{T}_{\text{train}}[1]$ , we assume that the source transmits a known pilot signal and the relay remains silent, while, for all  $t \in \mathcal{T}_{\text{train}}[2]$ , the relay transmits and the source remains silent. Moreover, we construct the pilot sequence  $\mathbf{X} = [\mathbf{x}(1), \dots, \mathbf{x}(TN)] \in \mathbb{C}^{N \times TN}$  to satisfy  $\frac{1}{2T} \mathbf{X} \mathbf{X}^H = \mathbf{I}_N$ , where the scaling has been chosen to satisfy a per-period power constraint of the form  $\text{tr}(\mathbf{Q}) = 2$ , consistent with the data power constraints that will be described in the sequel.

Our limited transmitter/receiver-DR model implies that the (distorted) space-time pilot signal observed by a given receiver takes the form

$$\mathbf{Y} = \sqrt{\alpha} \mathbf{H}(\mathbf{X} + \mathbf{C}) + \mathbf{N} + \mathbf{E}, \quad (5)$$

where  $\alpha \in \{\rho_r, \eta_r, \rho_d, \eta_d\}$  for  $\mathbf{H} \in \{\mathbf{H}_{sr}, \mathbf{H}_{rr}, \mathbf{H}_{rd}, \mathbf{H}_{sd}\}$ , respectively. In (5),  $\mathbf{C}, \mathbf{E}$  and  $\mathbf{N}$  are  $N \times TN$  matrices of transmitter noise, receiver distortion, and AWGN, respectively. At the conclusion of training, we assume that each receiver uses least-squares (LS) to estimate the corresponding channel  $\mathbf{H}$  as

$$\sqrt{\alpha} \hat{\mathbf{H}} \triangleq \frac{1}{2T} \mathbf{Y} \mathbf{X}^H, \quad (6)$$



and communicates this estimate to the transmitter.<sup>2</sup> In the sequel, it will be useful to decompose the channel estimate into the true channel plus an estimation error. In Appendix A, it is shown that such a decomposition takes the form

$$\sqrt{\alpha}\hat{\mathbf{H}} = \sqrt{\alpha}\mathbf{H} + \mathbf{D}^{\frac{1}{2}}\tilde{\mathbf{H}}, \quad (7)$$

where the entries of  $\tilde{\mathbf{H}}$  are i.i.d  $\mathcal{CN}(0, 1)$ , and where

$$\mathbf{D} = \frac{1}{2T} \left( (1 + \beta)\mathbf{I} + \alpha \frac{2\kappa}{N} \mathbf{H}\mathbf{H}^H + \alpha \frac{2\beta}{N} (1 + \kappa) \text{diag}(\mathbf{H}\mathbf{H}^H) \right) \quad (8)$$

characterizes the spatial covariance of the estimation error. Using  $\beta \ll 1$  and  $\kappa \ll 1$ , this covariance reduces to

$$\mathbf{D} \approx \frac{1}{2T} \left( \mathbf{I} + \alpha \frac{2\kappa}{N} \mathbf{H}\mathbf{H}^H + \alpha \frac{2\beta}{N} \text{diag}(\mathbf{H}\mathbf{H}^H) \right). \quad (9)$$

### B. Interference Cancellation and Equivalent Channel

We now describe how the relay partially cancels its self-interference, and construct a simplified model for the result.

Recall that the data communication period is partitioned into two periods,  $\mathcal{T}_{\text{data}}[1]$  and  $\mathcal{T}_{\text{data}}[2]$ , and that—within each—the transmitted signals are wide-sense stationary. Thus, at any time  $t \in \mathcal{T}_{\text{data}}[l]$ , the relay's (instantaneous, distorted) observed signal takes the form

$$\mathbf{y}_r(t) = (\sqrt{\rho_r}\hat{\mathbf{H}}_{\text{sr}} - \mathbf{D}_{\text{sr}}^{\frac{1}{2}}\tilde{\mathbf{H}}_{\text{sr}})(\mathbf{x}_s(t) + \mathbf{c}_s(t)) + \mathbf{n}_r(t) + \mathbf{e}_r(t) + (\sqrt{\eta_r}\hat{\mathbf{H}}_{\text{rr}} - \mathbf{D}_{\text{rr}}^{\frac{1}{2}}\tilde{\mathbf{H}}_{\text{rr}})(\mathbf{x}_r(t) + \mathbf{c}_r(t)), \quad (10)$$

as implied by Fig. 2 and (7). Defining the aggregate noise term

$$\mathbf{v}_r(t) \triangleq \sqrt{\rho_r}\hat{\mathbf{H}}_{\text{sr}}\mathbf{c}_s(t) - \mathbf{D}_{\text{sr}}^{\frac{1}{2}}\tilde{\mathbf{H}}_{\text{sr}}(\mathbf{x}_s(t) + \mathbf{c}_s(t)) + \mathbf{n}_r(t) + \mathbf{e}_r(t) + \sqrt{\eta_r}\hat{\mathbf{H}}_{\text{rr}}\mathbf{c}_r(t) - \mathbf{D}_{\text{rr}}^{\frac{1}{2}}\tilde{\mathbf{H}}_{\text{rr}}(\mathbf{x}_r(t) + \mathbf{c}_r(t)), \quad (11)$$

we can write the observed signal as  $\mathbf{y}_r(t) = \sqrt{\rho_r}\hat{\mathbf{H}}_{\text{sr}}\mathbf{x}_s(t) + \sqrt{\eta_r}\hat{\mathbf{H}}_{\text{rr}}\mathbf{x}_r(t) + \mathbf{v}_r(t)$ , where the self-interference term  $\sqrt{\eta_r}\hat{\mathbf{H}}_{\text{rr}}\mathbf{x}_r(t)$  is known and thus can be canceled. The interference-canceled signal  $\mathbf{z}_r(t) \triangleq \mathbf{y}_r(t) - \sqrt{\eta_r}\hat{\mathbf{H}}_{\text{rr}}\mathbf{x}_r(t)$  can then be written as

$$\mathbf{z}_r(t) = \sqrt{\rho_r}\hat{\mathbf{H}}_{\text{sr}}\mathbf{x}_s(t) + \mathbf{v}_r(t). \quad (12)$$

Equation (12) shows that, in effect, the information signal  $\mathbf{x}_s(t)$  propagates through a known channel  $\sqrt{\rho_r}\hat{\mathbf{H}}_{\text{sr}}$  corrupted by an aggregate (possibly non-Gaussian) noise  $\mathbf{v}_r(t)$ , whose  $(\hat{\mathbf{H}}_{\text{sr}}, \hat{\mathbf{H}}_{\text{rr}})$ -conditional covariance we denote as  $\hat{\Sigma}_r[l] \triangleq \text{Cov}\{\mathbf{v}_r(t) | \hat{\mathbf{H}}_{\text{sr}}, \hat{\mathbf{H}}_{\text{rr}}\}_{t \in \mathcal{T}_{\text{data}}[l]}$ , recalling that  $l \in \{1, 2\}$  indexes the data-period. In Appendix B, we show that

$$\begin{aligned} \hat{\Sigma}_r[l] &\approx \mathbf{I} + \kappa\rho_r\hat{\mathbf{H}}_{\text{sr}}\text{diag}(\mathbf{Q}_s[l])\hat{\mathbf{H}}_{\text{sr}}^H + \hat{\mathbf{D}}_{\text{sr}}\text{tr}(\mathbf{Q}_s[l]) \\ &\quad + \kappa\eta_r\hat{\mathbf{H}}_{\text{rr}}\text{diag}(\mathbf{Q}_r[l])\hat{\mathbf{H}}_{\text{rr}}^H + \hat{\mathbf{D}}_{\text{rr}}\text{tr}(\mathbf{Q}_r[l]) \\ &\quad + \beta\rho_r\text{diag}(\hat{\mathbf{H}}_{\text{sr}}\mathbf{Q}_s[l]\hat{\mathbf{H}}_{\text{sr}}^H) \\ &\quad + \beta\eta_r\text{diag}(\hat{\mathbf{H}}_{\text{rr}}\mathbf{Q}_r[l]\hat{\mathbf{H}}_{\text{rr}}^H), \end{aligned} \quad (13)$$

<sup>2</sup> In our transmission protocol, a single training epoch is followed by a large number of data epochs, and so the relative training overhead becomes negligible as the number of data epochs grows large.

where  $\hat{\mathbf{D}}_{\text{sr}} \triangleq \mathbb{E}\{\mathbf{D}_{\text{sr}} | \hat{\mathbf{H}}_{\text{sr}}\}$  and  $\hat{\mathbf{D}}_{\text{rr}} \triangleq \mathbb{E}\{\mathbf{D}_{\text{rr}} | \hat{\mathbf{H}}_{\text{rr}}\}$  obey

$$\hat{\mathbf{D}} \approx \frac{1}{2T} \left( \mathbf{I} + \alpha \frac{2\kappa}{N} \hat{\mathbf{H}}\hat{\mathbf{H}}^H + \alpha \frac{2\beta}{N} \text{diag}(\hat{\mathbf{H}}\hat{\mathbf{H}}^H) \right) \quad (14)$$

and where the approximations in (13)-(14) follow from  $\kappa \ll 1$  and  $\beta \ll 1$ . We note, for later use, that the channel estimation error terms  $\hat{\mathbf{D}}$  can be made arbitrarily small through appropriate choice of  $T$ .

The effective channel from the relay to the destination can be similarly stated as

$$\mathbf{y}_d(t) = \sqrt{\rho_d}\hat{\mathbf{H}}_{\text{rd}}\mathbf{x}_r(t) + \mathbf{v}_d(t) \quad (15)$$

$$\begin{aligned} \mathbf{v}_d(t) &\triangleq \sqrt{\rho_d}\hat{\mathbf{H}}_{\text{rd}}\mathbf{c}_r(t) - \mathbf{D}_{\text{rd}}^{\frac{1}{2}}\tilde{\mathbf{H}}_{\text{rd}}\mathbf{x}_r(t) + \mathbf{n}_d(t) + \mathbf{e}_d(t) \\ &\quad + \sqrt{\eta_d}\hat{\mathbf{H}}_{\text{sd}}(\mathbf{x}_s(t) + \mathbf{c}_s(t)) - \mathbf{D}_{\text{sd}}^{\frac{1}{2}}\tilde{\mathbf{H}}_{\text{sd}}(\mathbf{x}_s(t) + \mathbf{c}_s(t)), \end{aligned} \quad (16)$$

and an expression similar to (13) can be derived for the destination's aggregate noise covariance,  $\hat{\Sigma}_d[l] \triangleq \text{Cov}\{\mathbf{v}_d(t) | \hat{\mathbf{H}}_{\text{rd}}, \hat{\mathbf{H}}_{\text{sd}}\}_{t \in \mathcal{T}_{\text{data}}[l]}$  during data-period  $l \in \{1, 2\}$ . Unlike the relay node, however, the destination node does not cancel the interference term  $\sqrt{\eta_d}\hat{\mathbf{H}}_{\text{sd}}\mathbf{x}_s(t)$ , but rather lumps it in with the aggregate noise  $\mathbf{v}_d(t)$ . The latter practice is well motivated under the assumption that  $\eta_d \ll \rho_r$ , i.e., that the source-to-destination link is much weaker than the relay-to-destination link. Figure 3 summarizes the equivalent system model.

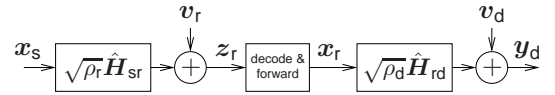


Fig. 3. Equivalent model of full-duplex MIMO relaying.

### C. Bounds on Achievable Rate

The end-to-end mutual information can be written, for a given time-sharing parameter  $\tau$ , as [4]

$$I_\tau(\mathcal{Q}) = \min \left\{ \sum_{l=1}^2 \tau[l] I_{\text{sr}}(\mathcal{Q}[l]), \sum_{l=1}^2 \tau[l] I_{\text{rd}}(\mathcal{Q}[l]) \right\}, \quad (17)$$

where  $I_{\text{sr}}(\mathcal{Q}[l])$  and  $I_{\text{rd}}(\mathcal{Q}[l])$  are the period- $l$  mutual informations of the source-to-relay channel and relay-to-destination channel, respectively, and where  $\mathcal{Q}[l] \triangleq (\mathbf{Q}_s[l], \mathbf{Q}_r[l])$  and  $\mathcal{Q} \triangleq (\mathcal{Q}[1], \mathcal{Q}[2])$ .

To analyze  $I_{\text{sr}}(\mathcal{Q}[l])$  and  $I_{\text{rd}}(\mathcal{Q}[l])$ , we leverage the equivalent system model shown in Fig. 3, which includes channel-estimation error and relay-self-interference cancellation, and treats the source-to-destination link as a source of noise. The mutual-information analysis is, however, still complicated by the fact that the aggregate noises  $\mathbf{v}_r(t)$  and  $\mathbf{v}_d(t)$  are generally non-Gaussian, as a result of the channel-estimation-error components in (11) and (16). However, it is known that, among all noise distributions of a given covariance, the Gaussian one is worst from a mutual-information perspective [20]. In particular, treating the noise as Gaussian yields the lower

bounds  $I_{\text{sr}}(\mathbf{Q}[l]) \geq \underline{I}_{\text{sr}}(\mathbf{Q}[l])$  and  $I_{\text{rd}}(\mathbf{Q}[l]) \geq \underline{I}_{\text{rd}}(\mathbf{Q}[l])$ , where [21]

$$\underline{I}_{\text{sr}}(\mathbf{Q}[l]) = \log \det \left( \mathbf{I} + \rho_r \hat{\mathbf{H}}_{\text{sr}} \mathbf{Q}_{\text{s}}[l] \hat{\mathbf{H}}_{\text{sr}}^H \hat{\Sigma}_{\text{r}}^{-1}[l] \right) \quad (18)$$

$$= \log \det \left( \rho_r \hat{\mathbf{H}}_{\text{sr}} \mathbf{Q}_{\text{s}}[l] \hat{\mathbf{H}}_{\text{sr}}^H + \hat{\Sigma}_{\text{r}}[l] \right) - \log \det(\hat{\Sigma}_{\text{r}}[l]) \quad (19)$$

and

$$\underline{I}_{\text{rd}}(\mathbf{Q}[l]) = \log \det \left( \mathbf{I} + \rho_d \hat{\mathbf{H}}_{\text{rd}} \mathbf{Q}_{\text{r}}[l] \hat{\mathbf{H}}_{\text{rd}}^H \hat{\Sigma}_{\text{r}}^{-1}[l] \right) \quad (20)$$

$$= \log \det \left( \rho_d \hat{\mathbf{H}}_{\text{rd}} \mathbf{Q}_{\text{r}}[l] \hat{\mathbf{H}}_{\text{rd}}^H + \hat{\Sigma}_{\text{d}}[l] \right) - \log \det(\hat{\Sigma}_{\text{d}}[l]), \quad (21)$$

and thus a lower bound on the end-to-end  $\tau$ -specific achievable-rate is

$$\underline{I}_{\tau}(\mathbf{Q}) = \min \left\{ \underbrace{\sum_{l=1}^2 \tau[l] \underline{I}_{\text{sr}}(\mathbf{Q}[l])}_{\triangleq \underline{I}_{\text{sr},\tau}(\mathbf{Q})}, \underbrace{\sum_{l=1}^2 \tau[l] \underline{I}_{\text{rd}}(\mathbf{Q}[l])}_{\triangleq \underline{I}_{\text{rd},\tau}(\mathbf{Q})} \right\}. \quad (22)$$

Moreover, the rate  $\underline{I}_{\tau}(\mathbf{Q})$  bits<sup>3</sup>-per-channel-use (bpcu) can be achieved via independent Gaussian codebooks at the transmitters and maximum-likelihood detection at the receivers [21].

A straightforward achievable-rate upper bound  $\bar{I}_{\tau}(\mathbf{Q})$  results from the case of perfect CSI (i.e.,  $\hat{\mathbf{D}} = \mathbf{0}$ ), where  $\mathbf{v}_{\text{r}}(t)$  and  $\mathbf{v}_{\text{d}}(t)$  are Gaussian. Moreover, the lower bound  $\underline{I}_{\tau}(\mathbf{Q})$  converges to the upper bound  $\bar{I}_{\tau}(\mathbf{Q})$  as the training  $T \rightarrow \infty$ .

#### IV. TRANSMIT COVARIANCE OPTIMIZATION

We would now like to find the transmit covariance matrices  $\mathbf{Q}$  that maximize the achievable-rate lower bound  $\underline{I}_{\tau}(\mathbf{Q})$  in (22) subject to the per-link power constraint  $\mathbf{Q} \in \mathbb{Q}_{\tau}$ , where

$$\mathbb{Q}_{\tau} \triangleq \left\{ \mathbf{Q} \text{ s.t. } \sum_{l=1}^2 \tau[l] \text{tr}(\mathbf{Q}_{\text{s}}[l]) \leq 1, \sum_{l=1}^2 \tau[l] \text{tr}(\mathbf{Q}_{\text{r}}[l]) \leq 1, \right. \\ \left. \mathbf{Q}_{\text{s}}[l] = \mathbf{Q}_{\text{s}}^H[l] \geq 0, \mathbf{Q}_{\text{r}}[l] = \mathbf{Q}_{\text{r}}^H[l] \geq 0 \right\}, \quad (23)$$

and subsequently optimize the time-sharing parameter  $\tau$ . We note that optimizing the transmit covariance matrices is equivalent to jointly optimizing the transmission beam-patterns and power levels. In the sequel, we denote the optimal (i.e., maximin) rate, for a given  $\tau$ , by

$$\underline{I}_{*,\tau} \triangleq \max_{\mathbf{Q} \in \mathbb{Q}_{\tau}} \min \{ \underline{I}_{\text{sr},\tau}(\mathbf{Q}), \underline{I}_{\text{rd},\tau}(\mathbf{Q}) \}, \quad (24)$$

and we use  $\mathbb{Q}_{*,\tau}$  to denote the corresponding set of maximin covariance designs  $\mathbf{Q}$  (which are, in general, not unique). Then, with  $\tau_* \triangleq \arg \max_{\tau \in [0,1]} \underline{I}_{*,\tau}$ , the optimal rate is  $\underline{I}_* \triangleq \underline{I}_{*,\tau_*}$ , and the corresponding set of maximin designs is  $\mathbf{Q}_* \triangleq \mathbb{Q}_{*,\tau_*}$ .

<sup>3</sup> Throughout the paper, we take “log” to be base-2.

#### A. Weighted-Sum-Rate Optimization

It is important to realize that, within the maximin design set  $\mathbb{Q}_{*,\tau}$ , there exists at least one “link-equalizing” design, i.e.,  $\exists \mathbf{Q} \in \mathbb{Q}_{*,\tau}$  s.t.  $\underline{I}_{\text{sr},\tau}(\mathbf{Q}) = \underline{I}_{\text{rd},\tau}(\mathbf{Q})$ . To see why this is the case, notice that, given any maximin design  $\mathbf{Q}$  such that  $\underline{I}_{\text{sr},\tau}(\mathbf{Q}) > \underline{I}_{\text{rd},\tau}(\mathbf{Q})$ , a simple scaling of  $\mathbf{Q}_{\text{s}}[l]$  can yield  $\underline{I}_{\text{sr},\tau}(\mathbf{Q}) = \underline{I}_{\text{rd},\tau}(\mathbf{Q})$ , and thus an equalizing design. A similar argument can be made when  $\underline{I}_{\text{rd},\tau}(\mathbf{Q}) > \underline{I}_{\text{sr},\tau}(\mathbf{Q})$ .

Referring to the set of *all* link-equalizing designs (maximin or otherwise), for a given  $\tau$ , as

$$\mathbb{Q}_{=,\tau} \triangleq \{ \mathbf{Q} \in \mathbb{Q}_{\tau} \text{ s.t. } \underline{I}_{\text{sr},\tau}(\mathbf{Q}) = \underline{I}_{\text{rd},\tau}(\mathbf{Q}) \}, \quad (25)$$

the maximin equalizing design can be found by solving either  $\arg \max_{\mathbf{Q} \in \mathbb{Q}_{=,\tau}} \underline{I}_{\text{sr},\tau}(\mathbf{Q})$  or  $\arg \max_{\mathbf{Q} \in \mathbb{Q}_{=,\tau}} \underline{I}_{\text{rd},\tau}(\mathbf{Q})$ , where the equivalence is due to the equalizing property. More generally, the maximin equalizing design can be found by solving

$$\arg \max_{\mathbf{Q} \in \mathbb{Q}_{=,\tau}} \underline{I}_{\tau}(\mathbf{Q}, \zeta) \quad (26)$$

with any fixed  $\zeta \in [0, 1]$  and the  $\zeta$ -weighted sum-rate

$$\underline{I}_{\tau}(\mathbf{Q}, \zeta) \triangleq \zeta \underline{I}_{\text{sr},\tau}(\mathbf{Q}) + (1 - \zeta) \underline{I}_{\text{rd},\tau}(\mathbf{Q}). \quad (27)$$

To find the maximin equalizing design, we propose relaxing the constraint on  $\mathbf{Q}$  from  $\mathbb{Q}_{=,\tau}$  to  $\mathbb{Q}_{\tau}$ , yielding the  $\zeta$ -weighted-sum-rate optimization problem

$$\mathbf{Q}_{*,\tau}(\zeta) = \arg \max_{\mathbf{Q} \in \mathbb{Q}_{\tau}} \underline{I}_{\tau}(\mathbf{Q}, \zeta). \quad (28)$$

Now, if there exists  $\zeta_{=} \in [0, 1]$  such that the solution  $\mathbf{Q}_{*,\tau}(\zeta_{=})$  to (28) is link-equalizing, then, because  $\mathbb{Q}_{=,\tau} \subset \mathbb{Q}_{\tau}$ , we know that  $\mathbf{Q}_{*,\tau}(\zeta_{=})$  must also solve the problem (26), implying that  $\mathbf{Q}_{*,\tau}(\zeta_{=})$  is maximin. Figure 4(a) illustrates the case where such a  $\zeta_{=}$  exists. It may be, however, that no  $\zeta \in [0, 1]$  yields a link-equalizing solution  $\mathbf{Q}_{*,\tau}(\zeta)$ , as illustrated in Fig. 4(b). This case occurs when  $\underline{I}_{\text{sr},\tau}(\mathbf{Q}_{*,\tau}(\zeta)) > \underline{I}_{\text{rd},\tau}(\mathbf{Q}_{*,\tau}(\zeta))$  for all  $\zeta \in [0, 1]$ , such as when  $\rho_r \gg \rho_d$ . In this latter case, the maximin rate reduces to  $\underline{I}_{*,\tau} = \lim_{\zeta \rightarrow 0} \underline{I}_{\text{rd},\tau}(\mathbf{Q}_{*,\tau}(\zeta))$ .

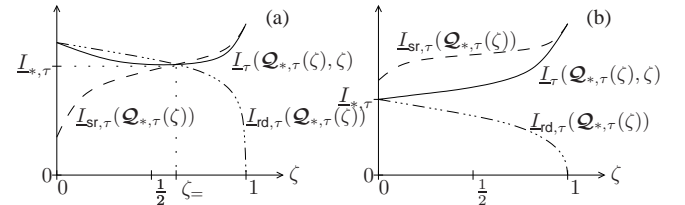


Fig. 4. Illustrative examples of  $\tau$ -specific  $\zeta$ -weighted sum-rate optimization in the case (a) when a link-equalizing solution exists and (b) when one does not exist. Here,  $\underline{I}_{\text{sr},\tau}(\mathbf{Q})$  and  $\underline{I}_{\text{rd},\tau}(\mathbf{Q})$  are the source-to-relay and relay-to-destination rates, respectively,  $\underline{I}_{\tau}(\mathbf{Q}, \zeta) = \zeta \underline{I}_{\text{sr},\tau}(\mathbf{Q}) + (1 - \zeta) \underline{I}_{\text{rd},\tau}(\mathbf{Q})$  is the  $\zeta$ -weighted sum-rate, and  $\mathbf{Q}_{*,\tau}(\zeta)$  is the set of optimal covariance matrices for a given time-share  $\tau$  and weight  $\zeta$ .

Whether or not  $\zeta_{=} \in [0, 1]$  actually exists, we propose to search for  $\zeta_{=}$  using bisection, leveraging the fact that  $\underline{I}_{\text{rd},\tau}(\mathbf{Q}_{*,\tau}(\zeta))$  is non-increasing in  $\zeta$  and  $\underline{I}_{\text{sr},\tau}(\mathbf{Q}_{*,\tau}(\zeta))$  is non-decreasing in  $\zeta$ . To perform the bisection search, we initialize the search interval  $\mathcal{I}$  at  $[0, 1]$ , and bisect it at each step after testing the condition  $\underline{I}_{\text{rd},\tau}(\mathbf{Q}_{*,\tau}(\zeta)) > \underline{I}_{\text{sr},\tau}(\mathbf{Q}_{*,\tau}(\zeta))$

at the midpoint location  $\zeta$  in  $\mathcal{I}$ ; if the condition holds true, we discard the left sub-interval of  $\mathcal{I}$ , else we discard the right sub-interval. We stop bisecting when  $|\underline{L}_{\text{d},\tau}(\mathbf{Q}_{*,\tau}(\zeta)) - \underline{L}_{\text{sr},\tau}(\mathbf{Q}_{*,\tau}(\zeta))|$  falls below a threshold or a maximum number of iterations has elapsed. Notice that, even when there exists no  $\zeta \in [0, 1]$ , bisection converges towards the desired weight  $\zeta = 0$ . Subsequently, we optimize over  $\tau \in [0, 1]$  using a grid-search.

### B. Gradient Projection

At each bisection step, we use Gradient Projection (GP) to solve<sup>4</sup> the  $\tau$ -specific,  $\zeta$ -weighted-sum-rate optimization problem (28). The GP algorithm [22] is defined as follows. For the generic problem of maximizing a function  $f(\mathbf{x})$  over  $\mathbf{x} \in \mathcal{X}$ , the GP algorithm starts with an initialization  $\mathbf{x}^{(0)}$  and iterates the following steps for  $k = 0, 1, 2, 3, \dots$

$$\tilde{\mathbf{x}}^{(k)} = \mathcal{P}_{\mathcal{X}}(\mathbf{x}^{(k)} + s^{(k)} \nabla f(\mathbf{x}^{(k)})) \quad (29)$$

$$\mathbf{x}^{(k+1)} = \mathbf{x}^{(k)} + \gamma^{(k)}(\tilde{\mathbf{x}}^{(k)} - \mathbf{x}^{(k)}), \quad (30)$$

where  $\mathcal{P}_{\mathcal{X}}(\cdot)$  denotes projection onto the set  $\mathcal{X}$  and  $\nabla f(\cdot)$  denotes the gradient of  $f(\cdot)$ . The parameters  $\gamma^{(k)} \in (0, 1]$  and  $s^{(k)}$  act as stepsizes. In the sequel, we assume  $s^{(k)} = 1 \forall k$ .

In applying GP to the optimization problem (28), we first take gradient steps for  $\mathbf{Q}_r[1]$  and  $\mathbf{Q}_r[2]$ , and then project onto the constraint set (23). Next, we take gradient steps for  $\mathbf{Q}_s[1]$  and  $\mathbf{Q}_s[2]$ , and then project onto the constraint set. In summary, denoting the relay gradient by  $\mathbf{G}_r[l] \triangleq \nabla_{\mathbf{Q}_r[l]} \underline{L}_{\tau}(\mathbf{Q}, \zeta)$ , our GP algorithm iterates the following steps to convergence:

$$\mathbf{P}_r^{(k)}[1] = \mathbf{Q}_r^{(k)}[1] + \mathbf{G}_r^{(k)}[1] \quad (31)$$

$$\mathbf{P}_r^{(k)}[2] = \mathbf{Q}_r^{(k)}[2] + \mathbf{G}_r^{(k)}[2] \quad (32)$$

$$(\tilde{\mathbf{Q}}_r^{(k)}[1], \tilde{\mathbf{Q}}_r^{(k)}[2]) = \mathcal{P}_{\mathcal{X}}(\mathbf{P}_r^{(k)}[1], \mathbf{P}_r^{(k)}[2]) \quad (33)$$

$$\mathbf{Q}_r^{(k+1)}[1] = \mathbf{Q}_r^{(k)}[1] + \gamma^{(k)}(\tilde{\mathbf{Q}}_r^{(k)}[1] - \mathbf{Q}_r^{(k)}[1]) \quad (34)$$

$$\mathbf{Q}_r^{(k+1)}[2] = \mathbf{Q}_r^{(k)}[2] + \gamma^{(k)}(\tilde{\mathbf{Q}}_r^{(k)}[2] - \mathbf{Q}_r^{(k)}[2]) \quad (35)$$

and then repeats similar steps for  $\mathbf{Q}_s[1]$  and  $\mathbf{Q}_s[2]$ . An outer loop then repeats this pair of inner loops until the maximum change in  $\mathbf{Q}$  is below a small positive threshold  $\epsilon$ .

We now provide additional details on the GP steps. As for the gradient, Appendix C shows that the gradient  $\mathbf{G}_r[l]$  can be written as in (36), at the top of the next page, where

$$\mathbf{S}_d[l] \triangleq \rho_d \hat{\mathbf{H}}_{\text{rd}} \mathbf{Q}_r[l] \hat{\mathbf{H}}_{\text{rd}}^H + \hat{\Sigma}_d[l] \quad (37)$$

$$\mathbf{S}_r[l] \triangleq \rho_r \hat{\mathbf{H}}_{\text{sr}} \mathbf{Q}_s[l] \hat{\mathbf{H}}_{\text{sr}}^H + \hat{\Sigma}_r[l]. \quad (38)$$

For  $\mathbf{G}_s[l]$ , a similar expression can be derived.

To compute the projection  $\mathcal{P}_{\mathcal{X}}(\mathbf{P}_r[1], \mathbf{P}_r[2])$ , we first notice that, due to the Hermitian property of  $\mathbf{P}_r[l]$ , we can construct an eigenvalue decomposition  $\mathbf{P}_r[l] = \mathbf{U}_r[l] \mathbf{\Lambda}_r[l] \mathbf{U}_r^H[l]$  with unitary  $\mathbf{U}_r[l]$  and real-valued  $\mathbf{\Lambda}_r[l] = \text{Diag}(\lambda_{r,1}[l], \lambda_{r,2}[l], \dots, \lambda_{r,N}[l])$ . The projection of  $(\mathbf{P}_r[1], \mathbf{P}_r[2])$  onto the constraint set (23)

then equals  $\tilde{\mathbf{Q}}_r[l] = \mathbf{U}_r[l](\mathbf{\Lambda}_r[l] - \mu \mathbf{I})^+ \mathbf{U}_r^H[l]$ , where  $(\mathbf{B})^+ = \max(\mathbf{B}, \mathbf{0})$  elementwise, and where  $\mu$  is chosen such that  $\sum_{n=1}^N \sum_{l=1}^2 \tau[l] \max(\lambda_{r,n}[l] - \mu, 0) = 1$ . In essence,  $\mathcal{P}_{\mathcal{X}}(\cdot)$  performs water-filling.

To adjust the stepsize  $\gamma^{(k)}$ , we use the Armijo stepsize rule [22], i.e.,  $\gamma^{(k)} = \nu^{m_k}$  where  $m_k$  is the smallest nonnegative integer that satisfies

$$\begin{aligned} & \underline{L}_{\tau}(\mathbf{Q}^{(k+1)}, \zeta) - \underline{L}_{\tau}(\mathbf{Q}^{(k)}, \zeta) \\ & \geq \sigma \nu^{m_k} \sum_{l=1}^2 \text{tr} \left( \mathbf{G}_s^{(k)H}[l] (\tilde{\mathbf{Q}}_s^{(k)}[l] - \mathbf{Q}_s^{(k)}[l]) \right. \\ & \quad \left. + \mathbf{G}_r^{(k)H}[l] (\tilde{\mathbf{Q}}_r^{(k)}[l] - \mathbf{Q}_r^{(k)}[l]) \right) \end{aligned} \quad (39)$$

for some constants  $\sigma, \nu$  typically chosen so that  $\sigma \in [10^{-5}, 10^{-1}]$  and  $\nu \in [0.1, 0.5]$ . Above, we used the shorthand  $\mathbf{Q}^{(k)} \triangleq (\mathbf{Q}_s^{(k)}[1], \mathbf{Q}_s^{(k)}[2], \mathbf{Q}_r^{(k)}[1], \mathbf{Q}_r^{(k)}[2])$ .

### V. ACHIEVABLE-RATE APPROXIMATION

The complicated nature of the optimization problem (24) motivates us to approximate its solution, i.e., the covariance-optimized achievable rate  $\underline{L}_* = \max_{\tau \in [0, 1]} \max_{\mathbf{Q} \in \mathcal{Q}_{\tau}} \underline{L}_{\tau}(\mathbf{Q})$ . In doing so, we focus on the case of  $T \rightarrow \infty$ , where channel estimation error is driven to zero so that  $\underline{L}_{\tau}(\mathbf{Q}) = \bar{L}_{\tau}(\mathbf{Q})$ . In addition, for tractability, we restrict ourselves to the case  $N_s = N_r = N$  and  $M_r = M_d = M$  (i.e.,  $N$  transmit antennas and  $M$  receive antennas at each node), the case  $\eta_d = 0$  (i.e., no direct source-to-destination link), and the case  $\tau = \frac{1}{2}$  (i.e., equal time-sharing).

Our approximation is built around the simplifying case that the channel matrices  $\{\mathbf{H}_{\text{sr}}, \mathbf{H}_{\text{rr}}, \mathbf{H}_{\text{rd}}\}$  are each diagonal, although not necessarily square, and have  $R \triangleq \min\{M, N\}$  identical diagonal entries equal to  $\sqrt{MN/R}$ . (The latter value is chosen so that  $\mathbb{E}\{\text{tr}(\mathbf{H}\mathbf{H}^H)\} = MN$  as assumed in Section II-A.) In this case, the mutual information (22) becomes (40), at the top of the next page. When  $\eta_r \ll \rho_r$ , the  $\eta_r$ -dependent terms in (40) can be ignored, after which it is straightforward to show that, under the constraint (23), the optimal covariances are the “full duplex”  $\mathbf{Q}_{\text{FD}} \triangleq (\frac{1}{N}\mathbf{I}, \frac{1}{N}\mathbf{I}, \frac{1}{N}\mathbf{I}, \frac{1}{N}\mathbf{I})$ , for which (40) gives

$$\begin{aligned} & I(\mathbf{Q}_{\text{FD}}) \\ & \approx R \log \left( 1 + \min \left\{ \frac{\rho_r}{\frac{R}{M} + (\kappa + \beta)(\rho_r + \eta_r)}, \frac{\rho_d}{\frac{R}{M} + (\kappa + \beta)\rho_d} \right\} \right) \end{aligned} \quad (41)$$

$$= \begin{cases} R \log \left( 1 + \frac{\rho_d}{\frac{R}{M} + (\kappa + \beta)\rho_d} \right) & \text{if } \frac{\rho_r}{\rho_d} \geq 1 + \frac{(\kappa + \beta)\eta_r M}{R} \\ R \log \left( 1 + \frac{\rho_r}{\frac{R}{M} + (\kappa + \beta)(\rho_r + \eta_r)} \right) & \text{else.} \end{cases} \quad (42)$$

When  $\eta_r \gg \rho_r$ , the  $\eta_r$ -dependent term in (40) dominates unless  $\mathbf{Q}_r[l] = \mathbf{0}$ . In this case, the optimal covariances are the “half duplex” ones  $\mathbf{Q}_{\text{HD}} \triangleq (\frac{2}{N}\mathbf{I}, \mathbf{0}, \mathbf{0}, \frac{2}{N}\mathbf{I})$ , for which (40) gives

$$I(\mathbf{Q}_{\text{HD}}) \approx \begin{cases} \frac{R}{2} \log \left( 1 + \frac{\rho_d}{\frac{R}{2M} + (\kappa + \beta)\rho_d} \right) & \text{if } \frac{\rho_r}{\rho_d} \geq 1 \\ \frac{R}{2} \log \left( 1 + \frac{\rho_r}{\frac{R}{2M} + (\kappa + \beta)\rho_r} \right) & \text{else.} \end{cases} \quad (43)$$

Finally, given any triple  $(\rho_r, \eta_r, \rho_d)$ , we approximate the achievable rate as follows:  $I_* \approx \max\{I(\mathbf{Q}_{\text{FD}}), I(\mathbf{Q}_{\text{HD}})\}$ .

<sup>4</sup> Because (24) is generally non-convex, finding the global maximum can be difficult. Although GP is guaranteed only to find a local, and not global, maximum, our experience with different initializations suggests that GP is indeed finding the global maximum in our problem.

$$\begin{aligned}
\frac{\mathbf{G}_r[l]}{2\tau[l]} = & \frac{(1-\zeta)\rho_d}{\ln 2} \left\{ \hat{\mathbf{H}}_{rd}^H \left( \mathbf{S}_d^{-1}[l] + \beta \text{diag}(\mathbf{S}_d^{-1}[l] - \hat{\Sigma}_d^{-1}[l]) \right) \hat{\mathbf{H}}_{rd} + \text{diag} \left( \kappa \hat{\mathbf{H}}_{rd}^H (\mathbf{S}_d^{-1}[l] - \hat{\Sigma}_d^{-1}[l]) \hat{\mathbf{H}}_{rd} \right) \right\} \\
& + \frac{1-\zeta}{\ln 2} \text{sum} \left( \hat{\mathbf{D}}_{rd}^* \odot (\mathbf{S}_d^{-1}[l] - \hat{\Sigma}_d^{-1}[l]) \right) \mathbf{I} + \frac{\zeta}{\ln 2} \text{sum} \left( \hat{\mathbf{D}}_{rr}^* \odot (\mathbf{S}_r^{-1}[l] - \hat{\Sigma}_r^{-1}[l]) \right) \mathbf{I} \\
& + \frac{\zeta\eta_r}{\ln 2} \left\{ \text{diag} \left( \kappa \hat{\mathbf{H}}_{rr}^H (\mathbf{S}_r^{-1}[l] - \hat{\Sigma}_r^{-1}[l]) \hat{\mathbf{H}}_{rr} \right) + \beta \hat{\mathbf{H}}_{rd}^H \text{diag}(\mathbf{S}_r^{-1}[l] - \hat{\Sigma}_r^{-1}[l]) \hat{\mathbf{H}}_{rd} \right\}, \quad (36)
\end{aligned}$$

$$\begin{aligned}
I_\tau(\mathbf{Q}) \approx & \frac{1}{2} \min \left\{ \sum_{l=1}^2 \log \det \left( \mathbf{I} + \rho_r \frac{NM}{R} \mathbf{Q}_s[l] \left( \mathbf{I} + (\kappa + \beta) \frac{NM}{R} (\rho_r \text{diag}(\mathbf{Q}_s[l]) + \eta_r \text{diag}(\mathbf{Q}_r[l])) \right)^{-1} \right), \right. \\
& \left. \sum_{l=1}^2 \log \det \left( \mathbf{I} + \rho_d \frac{NM}{R} \mathbf{Q}_r[l] \left( \mathbf{I} + (\kappa + \beta) \frac{NM}{R} \rho_d \text{diag}(\mathbf{Q}_r[l]) \right)^{-1} \right) \right\}. \quad (40)
\end{aligned}$$

From (42)-(43), using  $\theta \triangleq \frac{R}{M(\kappa+\beta)}$ , it is straightforward to show that the approximated system operates as follows.

1) Say  $\frac{\rho_r}{\rho_d} \leq 1$ . Then full-duplex is used iff

$$\eta_r \leq \frac{1}{2} \sqrt{(\theta + 2\rho_r)^2 + \frac{2\rho_r}{\kappa + \beta}(\theta + 2\rho_r)} - \frac{1}{2}\theta. \quad (44)$$

For either half- or full-duplex,  $I_*$  is invariant to  $\rho_d$ , i.e., the source-to-relay link is the limiting one.

2) Say  $1 \leq \frac{\rho_r}{\rho_d} \leq 1 + \frac{(\kappa+\beta)\eta_r M}{R}$ . Full-duplex is used iff

$$\eta_r \leq \frac{\rho_r}{2\rho_d} \sqrt{(\theta + 2\rho_d)^2 + \frac{2\rho_d}{\kappa + \beta}(\theta + 2\rho_d)} - \theta \left( 1 - \frac{\rho_r}{2\rho_d} \right). \quad (45)$$

3) Say  $1 + \frac{(\kappa+\beta)\eta_r M}{R} \leq \frac{\rho_r}{\rho_d}$ , or equivalently  $\eta_r \leq \eta_{\text{crit}} \triangleq \left( \frac{\rho_r}{\rho_d} - 1 \right) \frac{R}{M(\kappa+\beta)}$ . Then full-duplex is always used, and  $I_*$  is invariant to  $\rho_r$  and  $\eta_r$ , i.e., the rate is limited by the relay-to-destination link.

Figure 5 shows a contour plot of the proposed achievable-rate approximation as a function of INR  $\eta_r$  and SNR  $\rho_r$ , for the case that  $\rho_r/\rho_d = 2$ . We shall see in Section VI that our approximation of the covariance-optimized achievable-rate is reasonably close to that found by solving (24) using bisection/GP.

## VI. NUMERICAL RESULTS

In this section, we numerically investigate the behavior of the end-to-end rates achievable for full-duplex MIMO relaying under the proposed limited transmitter/receiver-DR and channel-estimation-error models. Recall that, in Section III, it was shown that, for a fixed set of transmit covariance matrices  $\mathbf{Q}$  and time-sharing parameter  $\tau$ , the achievable rate  $I_\tau(\mathbf{Q})$  can be lower-bounded using  $\underline{I}_\tau(\mathbf{Q})$  from (22), and upper-bounded using the perfect-CSI  $\bar{I}_\tau(\mathbf{Q})$ , where the bounds converge as training  $T \rightarrow \infty$ . Then, in Section IV, a bisection/GP scheme was proposed to maximize  $\underline{I}_\tau(\mathbf{Q})$  subject to the power-constraint  $\mathbf{Q} \in \mathcal{Q}_\tau$ , which was subsequently maximized over  $\tau \in [0, 1]$ .

We now study the average behavior of the bisection/GP-optimized rate  $\underline{I}_* = \max_\tau \max_{\mathbf{Q} \in \mathcal{Q}_\tau} \underline{I}_\tau(\mathbf{Q})$  as a function of SNRs  $\rho_r$  and  $\rho_d$ ; INRs  $\eta_r$  and  $\eta_d$ ; dynamic range parameters

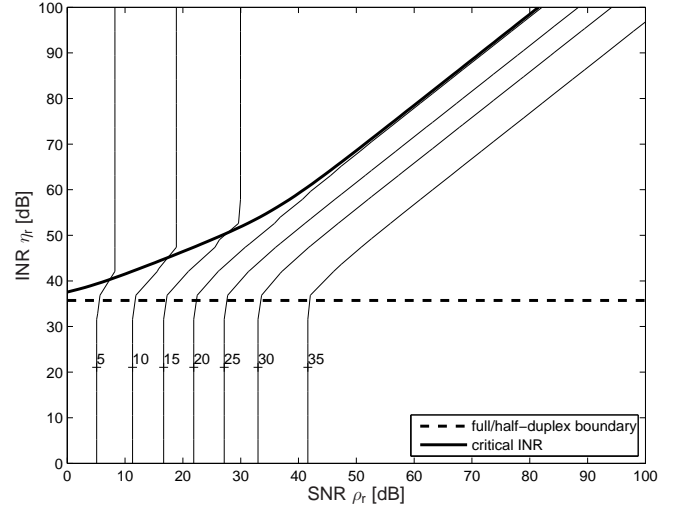


Fig. 5. Contour plot of the approximated achievable rate  $I_*$  versus relay SNR  $\rho_r$  and INR  $\eta_r$ , for  $N = 3$ ,  $M = 4$ ,  $\beta = \kappa = -40\text{dB}$ , and  $\rho_r/\rho_d = 2$ . The horizontal dashed line shows the INR  $\eta_{\text{crit}}$ , and the dark curve shows the boundary between full- and half-duplex regimes described in (45).

$\kappa$  and  $\beta$ ; number of antennas  $N_s$ ,  $N_r$ ,  $M_r$ , and  $M_d$ ; and training length  $T$ . We also investigate the role of interference cancellation, the role of two distinct data periods, the role of  $\tau$ -optimization, and the relation to optimized half-duplex (OHD) signaling. In doing so, we find close agreement with the achievable-rate approximation proposed in Section V and illustrated in Fig. 5.

For the numerical results below, the propagation channel model from Section II-A and the limited transmitter/receiver-DR models from Section II-C and Section II-D were employed, pilot-aided channel estimation was implemented as in Section III-A, and the power constraint (23) was applied, implying the channel-estimation-error covariance (8) and the aggregate-noise covariance (13). Throughout, we used  $N \triangleq N_s = N_r$  transmit antennas,  $M \triangleq M_r = M_d$  receive antennas, the SNR ratio  $\rho_r/\rho_d = 2$ , the destination INR  $\eta_d = 1$ , training duration  $T = 50$  (as justified below), Armijo parameters  $\sigma = 0.01$  and  $\nu = 0.2$ , and GP stopping threshold  $\epsilon = 0.01$ .



For each channel realization, the time-sharing coefficient  $\tau$  was optimized over the grid  $\tau \in \{0.1, 0.2, 0.3, \dots, 0.9\}$ , and all results were averaged over 100 realizations unless specified otherwise.

Below, we denote the full scheme proposed in Section IV by “TCO-2-IC,” which indicates the use of interference cancellation (IC) and transmit covariance optimization (TCO) performed individually over the 2 data periods (i.e.,  $\mathcal{T}_{\text{data}}[1]$  and  $\mathcal{T}_{\text{data}}[2]$ ). To test the impact of IC and of two data periods, we also implemented the proposed scheme but without IC, which we refer to as “TCO-2,” as well as the proposed scheme with only one data period (i.e.,  $\mathbf{Q}_i[1] = \mathbf{Q}_i[2] \forall i$ ), which we refer to as “TCO-1-IC.” To optimize<sup>5</sup> half-duplex, we used GP to maximize the sum-rate  $\underline{I}_\tau(\mathbf{Q}, \frac{1}{2})$  under the power constraint (23) and the half-duplex constraint  $\mathbf{Q}_1[2] = \mathbf{0} = \mathbf{Q}_2[1]$ ;  $\tau$ -optimization was performed as described above.

To mitigate GP’s sensitivity to initialization, we tried two initializations for each  $\zeta$ -weighted-sum-rate problem, OHD and “naive” full-duplex (NFD), and the one yielding the maximum min-rate was retained. OHD was calculated as explained above, whereas NFD employed non-zero OHD covariance matrices  $\mathbf{Q}_1[1]$  and  $\mathbf{Q}_2[2]$  over both data periods (which is indeed optimal when  $\eta_r = 0 = \eta_d$ ). Note that both OHD and NFD are invariant to  $\zeta$ ,  $\eta_r$ , and  $\eta_d$ .

In Fig. 6, we investigate the role of channel-estimation training length  $T$  on the achievable-rate lower bound  $\underline{I}(\mathbf{Q})$  of TCO-2-IC. There we see that the rate increases rapidly in  $T$  for small values of  $T$ , but quickly saturates for larger values of  $T$ . This behavior can be understood from (13)-(14), which suggest that channel estimation error will have a negligible effect on the noise covariances  $\hat{\Sigma}_r[l]$  and  $\hat{\Sigma}_d[l]$  when  $TN \gg 1$ . Figure 6 also shows the corresponding achievable-rate upper bounds  $\bar{I}(\mathbf{Q})$ . These traces confirm that the nominal training length  $T = 50$  ensures  $\underline{I}(\mathbf{Q}) \approx \bar{I}(\mathbf{Q}) \approx I(\mathbf{Q})$ .

In Fig. 7, we examine achievable-rate performance versus INR  $\eta_r$  for the TCO-2-IC, TCO-1-IC, TCO-2, and OHD schemes, using different dynamic range parameters  $\beta = \kappa$ . For OHD, we see that rate is invariant to INR  $\eta_r$ , as expected. For the proposed TCO-2-IC, we observe “full duplex” performance for low-to-mid values of  $\eta_r$  and a transition to OHD performance at high values of  $\eta_r$ , just as predicted by the approximation in Section V. In fact, the rates in Fig. 7 are very close to the approximated values in Fig. 5. To see the importance of two distinct data-communication periods, we examine the TCO-1-IC trace, where we observe TCO-2-IC-like performance at low-to-midrange values of  $\eta_r$ , but performance that drops below OHD at high  $\eta_r$ . Essentially, TCO-1-IC forces full-duplex signaling at high INR  $\eta_r$ , where half-duplex signaling is optimal, while TCO-2-IC facilitates the possibility of half-duplex signaling through the use of two distinct data-communication periods, similar to the MIMO-interference-channel scheme in [23]. The effect of  $\tau$ -

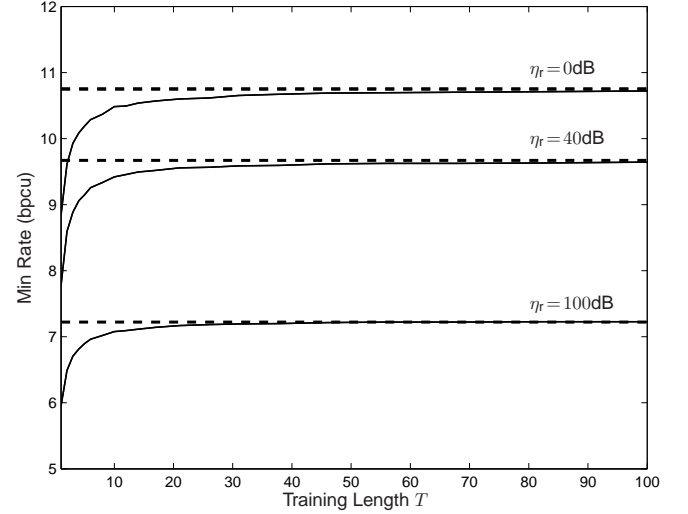


Fig. 6. Achievable-rate lower bound  $\underline{I}_*$  for TCO-2-IC versus training interval  $T$ . Here,  $N = 3$ ,  $M = 4$ ,  $\beta = \kappa = -40\text{dB}$ ,  $\rho_r = 15\text{dB}$ ,  $\rho_r/\rho_d = 2$ , and  $\eta_d = 0\text{dB}$ . Also shown as a dashed line which is the corresponding upper bound  $\bar{I}_*$  for each value of  $\eta_r$ .

optimization can be seen by comparing the two OHD traces, one which uses the fixed value  $\tau = 0.5$  and the other which uses the optimized value  $\tau = \tau_*$ . The separation between these traces shows that  $\tau$ -optimization gives a small but noticeable rate gain. Finally, by examining the TCO-2 trace, we conclude that partial interference cancellation is very important for all but extremely low or high values of INR  $\eta_r$ .

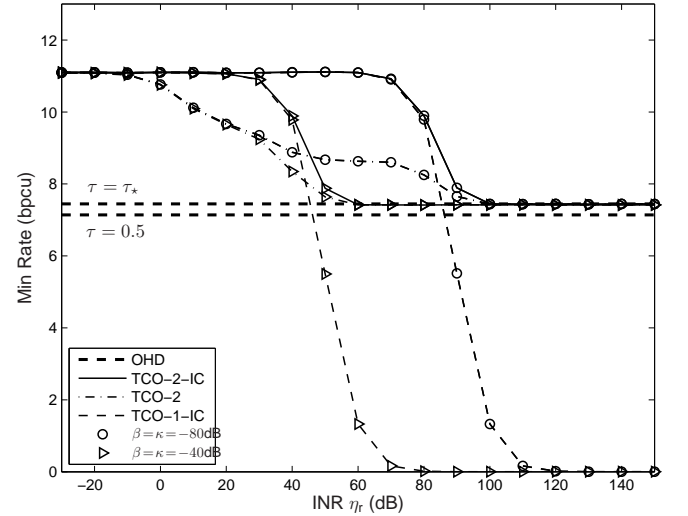


Fig. 7. Achievable-rate lower bound  $\underline{I}_*$  for TCO-2-IC, TCO-2, TCO-1-IC, and OHD versus INR  $\eta_r$ . Here,  $N = 3$ ,  $M = 4$ ,  $\rho_r = 15\text{dB}$ ,  $\rho_r/\rho_d = 2$ ,  $\eta_d = 0\text{dB}$ , and  $T = 50$ . OHD is plotted for  $\beta = \kappa = -40\text{dB}$ , but was observed to give nearly identical rate for  $\beta = \kappa = -80\text{dB}$ . Both fixed-time-share ( $\tau = 0.5$ ) and optimized-time-share ( $\tau = \tau_*$ ) versions of OHD are shown.

<sup>5</sup> We note that *both* half-duplex and the proposed TCO-2-IC scheme could potentially benefit from allowing the relay to change the partitioning of antennas from transmission to reception across the data period  $l \in \{1, 2\}$ . In half duplex mode, for example, it would be advantageous for the relay to use  $(N_r[1], M_r[1]) = (0, 7)$  and  $(N_r[2], M_r[2]) = (7, 0)$  as opposed to  $(N_r[l], M_r[l]) = (3, 4) \forall l$ . We do not consider such antenna-swapping in this work, however.

In Fig. 8, we examine the rate of the proposed TCO-IC-2 and OHD versus SNR  $\rho_r$ , using the dynamic range parameters  $\beta = \kappa = -40\text{dB}$ ,  $\eta_d = 0\text{dB}$ , and two fixed values of INR  $\eta_r$ . All the behaviors in Fig. 8 are predicted by the rate approximation described in Section V and illustrated in Fig. 5.



In particular, at the low INR of  $\eta_r = 20\text{dB}$ , TCO-IC-2 operates in the full-duplex regime for all values of SNR  $\rho_r$ . Meanwhile, at the high INR of  $\eta_r = 60\text{dB}$ , TCO-IC-2 operates in half-duplex at low values of SNR  $\rho_r$ , but switches to full-duplex after  $\rho_r$  exceeds a threshold.

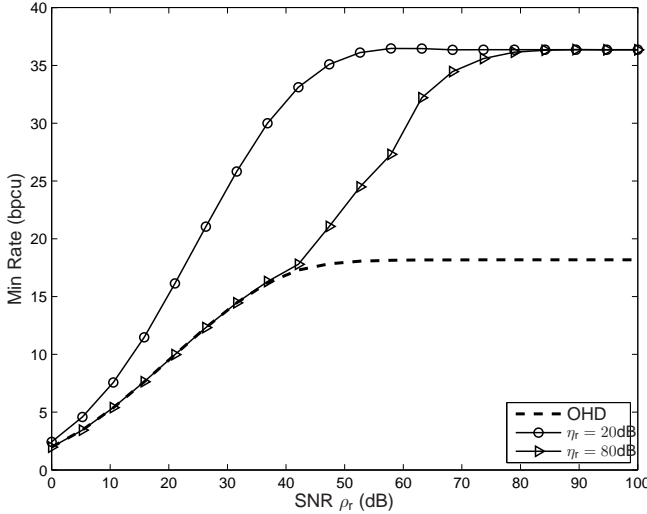


Fig. 8. Achievable-rate lower bound  $\underline{I}_*$  for TCO-2-IC and OHD versus SNR  $\rho_r$ . Here,  $\rho_r/\rho_d = 2$ ,  $\eta_d = 0\text{dB}$ ,  $N = 3$ ,  $M = 4$ ,  $\beta = \kappa = -40\text{dB}$ , and  $T = 50$ . OHD in this figure is optimized over  $\tau$ .

In Fig. 9, we plot the GP-optimized rate contours of the proposed TCO-IC-2 versus both SNR  $\rho_r$  and INR  $\eta_r$ , for comparison to the approximation in Fig. 5. The two plots show a relatively good match, confirming the accuracy of the approximation. The greatest discrepancy between the plots occurs when  $\eta_r \approx \rho_r$  and both  $\eta_r$  and  $\rho_r$  are large, which makes sense because the approximation was derived using  $\eta_r \ll \rho_r$  and  $\eta_r \gg \rho_r$ .

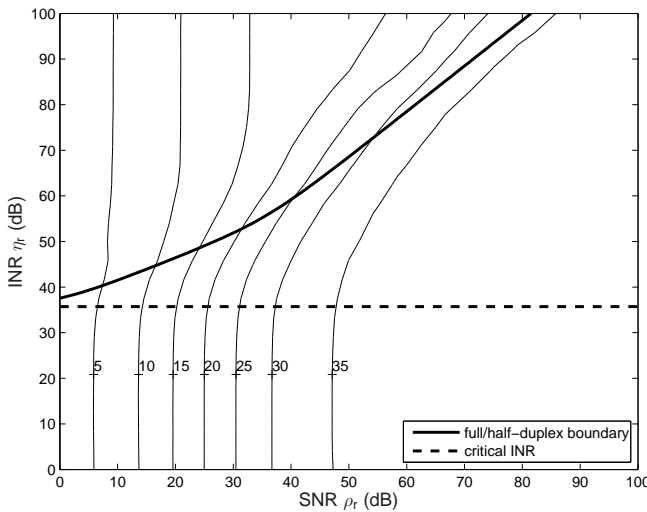


Fig. 9. Contour plot of the achievable-rate lower bound  $\underline{I}_*$  for TCO-2-IC versus INR  $\eta_r$  and SNR  $\rho_r$ , for  $\rho_d = \rho_r/2$ ,  $\eta_d = 0\text{dB}$ ,  $N = 3$ ,  $M = 4$ , and  $\beta = \kappa = -40\text{dB}$ . The dark curve (i.e., approximate full/half-duplex boundary) and dashed line (i.e., critical INR  $\eta_{\text{crit}}$ ) are the same as in Fig. 5, and shown for reference. The results are averaged over 250 realizations.

Finally, in Fig. 10, we explore the achievable rate of TCO-

2-IC and OHD versus the number of antennas,  $N$  and  $M$ , for fixed values of SNR  $\rho_r = 15\text{dB}$  and  $\rho_r/\rho_d = 2$ , INR  $\eta_r = 30\text{dB}$  and  $\eta_d = 0\text{dB}$ , and DR parameters  $\beta = \kappa = -40\text{dB}$ . We recall, from Fig. 7, that these parameters correspond to the interesting regime where TCO-2-IC performs between half- and full-duplex. In Fig. 10, we see that achievable rate increases with both  $M$  and  $N$  numbers of antennas, as expected. More interesting is the achievable-rate behavior when the total number of antennas per modem is fixed, e.g., at  $N + M = 7$ , as illustrated by the triangles in Fig. 10. The figure indicates that the configurations  $(N, M) = (3, 4)$  and  $(N, M) = (4, 3)$  are best, which (it can be shown) is consistent with approximation from Section V.

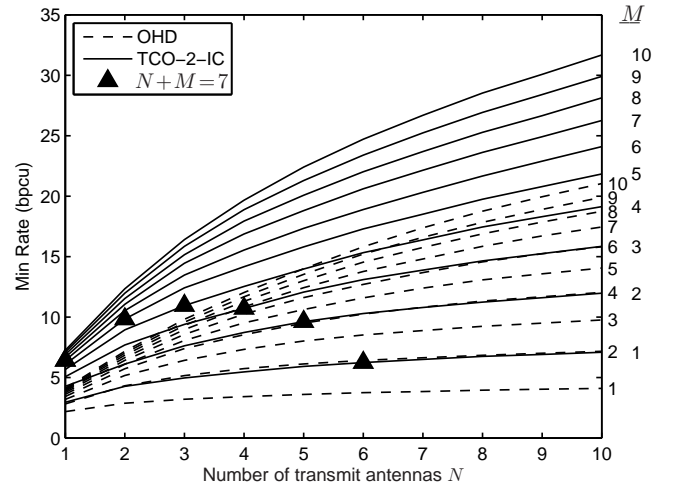


Fig. 10. Achievable-rate lower bound  $\underline{I}_*$  for TCO-2-IC and OHD versus number of transmit antennas  $N$  with various numbers of receive antennas  $M$ . Here,  $\rho_r = 15\text{dB}$ ,  $\rho_r/\rho_d = 2$ ,  $\eta_r = 30\text{dB}$ ,  $\eta_d = 0\text{dB}$ ,  $\beta = \kappa = -40\text{dB}$ , and  $T = 50$ . OHD shown in this figure is optimized over  $\tau$ .

## VII. CONCLUSION

We considered the problem of decode-and-forward-based full-duplex MIMO relaying between a source node and destination node. In our analysis, we considered limited transmitter/receiver dynamic range, imperfect CSI, background AWGN, and very high levels of self-interference. Using explicit models for dynamic-range limitation and pilot-aided channel estimation error, we derived upper and lower bounds on the end-to-end achievable rate that tighten as the number of pilots increases. Furthermore, we proposed a transmission scheme based on maximizing the achievable-rate lower-bound. The latter requires the solution to a nonconvex optimization problem, for which we use bisection search and Gradient Projection, the latter of which implicitly performs water-filling. In addition, we derived an analytic approximation to the achievable rate that agrees closely with the results of the numerical optimization. Finally, we studied the achievable-rate numerically, as a function of signal-to-noise ratio, interference-to-noise ratio, transmitter/receiver dynamic range, number of antennas, and number of pilots. In future work, we plan to investigate the effect of practical coding/decoding schemes, channel time-variation, and bidirectional relaying.

## APPENDIX A CHANNEL ESTIMATION DETAILS

In this appendix, we derive certain details of Section III-A. Under limited transmitter-DR, the undistorted received space-time signal is

$$\mathbf{U} = \sqrt{\alpha}\mathbf{H}(\mathbf{X} + \mathbf{C}) + \mathbf{N}, \quad (46)$$

where the spatial correlation<sup>6</sup> of the non-distorted pilot signal  $\mathbf{X}$  equals  $\frac{2}{N}\mathbf{I}$  and hence the spatial correlation of the transmitter distortion  $\mathbf{C}$  equals  $\frac{2\kappa}{N}\mathbf{I}$ . Conditioned on  $\mathbf{H}$ , the spatial correlation of  $\mathbf{U}$  is then  $\Phi = \frac{2\alpha(1+\kappa)}{N}\mathbf{H}\mathbf{H}^H + \mathbf{I}$ , and hence the  $\mathbf{H}$ -conditional spatial correlation of the receiver distortion  $\mathbf{E}$  equals

$$\beta \text{diag}(\Phi) = \beta \left( \frac{2\alpha(1+\kappa)}{N} \text{diag}(\mathbf{H}\mathbf{H}^H) + \mathbf{I} \right). \quad (47)$$

Given (5), the distorted received signal  $\mathbf{Y}$  can be written as

$$\mathbf{Y} = \sqrt{\alpha}\mathbf{H}\mathbf{X} + \mathbf{W}, \quad (48)$$

where  $\mathbf{W} \triangleq \sqrt{\alpha}\mathbf{H}\mathbf{C} + \mathbf{N} + \mathbf{E}$  is aggregate complex Gaussian noise that is temporally white with  $\mathbf{H}$ -conditional spatial correlation  $\frac{2\alpha\kappa}{N}\mathbf{H}\mathbf{H}^H + \mathbf{I} + \beta \left( \frac{2\alpha(1+\kappa)}{N} \text{diag}(\mathbf{H}\mathbf{H}^H) + \mathbf{I} \right)$ .

Due to the fact that  $\frac{1}{2T}\mathbf{X}\mathbf{X}^H = \mathbf{I}$ , the channel estimate (6) takes the form

$$\sqrt{\alpha}\hat{\mathbf{H}} = \frac{1}{2T}\mathbf{Y}\mathbf{X}^H = \sqrt{\alpha}\mathbf{H} + \frac{1}{2T}\mathbf{W}\mathbf{X}^H, \quad (49)$$

where  $\frac{1}{2T}\mathbf{W}\mathbf{X}^H$  is Gaussian channel estimation error. We now analyze the  $\mathbf{H}$ -conditional correlations among the elements of the channel estimation error matrix. We begin by noticing

$$\begin{aligned} & \mathbb{E} \left\{ \left[ \frac{1}{2T}\mathbf{W}\mathbf{X}^H \right]_{m,p} \left[ \frac{1}{2T}\mathbf{W}\mathbf{X}^H \right]_{n,q}^* \middle| \mathbf{H} \right\} \\ &= \frac{1}{(2T)^2} \mathbb{E} \left\{ \sum_k [\mathbf{W}]_{m,k} [\mathbf{X}]_{p,k}^* \sum_l [\mathbf{X}]_{q,l} [\mathbf{W}]_{n,l}^* \middle| \mathbf{H} \right\} \quad (50) \\ &= \frac{1}{(2T)^2} \sum_{k,l} [\mathbf{X}]_{p,k}^* [\mathbf{X}]_{q,l} \mathbb{E} \{ [\mathbf{W}]_{m,k} [\mathbf{W}]_{n,l}^* \mid \mathbf{H} \}. \quad (51) \end{aligned}$$

To find  $\mathbb{E} \{ [\mathbf{W}]_{m,k} [\mathbf{W}]_{n,l}^* \mid \mathbf{H} \}$ , we recall that

$$\mathbb{E} \{ [\mathbf{N}]_{m,k} [\mathbf{N}]_{n,l}^* \mid \mathbf{H} \} = \delta_{m-n} \delta_{k-l} \quad (52)$$

$$\mathbb{E} \{ [\mathbf{C}]_{q,k} [\mathbf{C}]_{p,l}^* \mid \mathbf{H} \} = \frac{2\kappa}{N} \delta_{q-p} \delta_{k-l} \quad (53)$$

$$\mathbb{E} \{ [\mathbf{E}]_{m,k} [\mathbf{E}]_{n,l}^* \mid \mathbf{H} \} = \beta [\Phi]_{m,m} \delta_{m-n} \delta_{k-l}, \quad (54)$$

implying that

$$\begin{aligned} & \mathbb{E} \{ [\mathbf{W}]_{m,k} [\mathbf{W}]_{n,l}^* \mid \mathbf{H} \} \\ &= \alpha \sum_{q,p} [\mathbf{H}]_{m,q} [\mathbf{H}]_{n,p}^* \mathbb{E} \{ [\mathbf{C}]_{q,k} [\mathbf{C}]_{p,l}^* \mid \mathbf{H} \} \\ &\quad + \mathbb{E} \{ [\mathbf{N}]_{m,k} [\mathbf{N}]_{n,l}^* \mid \mathbf{H} \} + \mathbb{E} \{ [\mathbf{E}]_{m,k} [\mathbf{E}]_{n,l}^* \mid \mathbf{H} \} \quad (55) \\ &= \delta_{k-l} \left( \alpha \frac{2\kappa}{N} \sum_p [\mathbf{H}]_{m,p} [\mathbf{H}]_{n,p}^* + (1 + \beta [\Phi]_{m,m}) \delta_{m-n} \right), \end{aligned}$$

<sup>6</sup> The spatial correlation of  $\mathbf{X} = [\mathbf{x}(1), \dots, \mathbf{x}(TN)]$  is  $\mathbb{E} \{ \mathbf{x}(t) \mathbf{x}(t)^H \} = \mathbb{E} \{ \frac{1}{TN} \sum_{t=1}^{TN} \mathbf{x}(t) \mathbf{x}(t)^H \} = \mathbb{E} \{ \frac{1}{TN} \mathbf{X} \mathbf{X}^H \}$ .

which implies that

$$\begin{aligned} & \mathbb{E} \left\{ \left[ \frac{1}{2T}\mathbf{W}\mathbf{X}^H \right]_{m,p} \left[ \frac{1}{2T}\mathbf{W}\mathbf{X}^H \right]_{n,q}^* \middle| \mathbf{H} \right\} \\ &= \frac{1}{(2T)^2} \sum_k [\mathbf{X}]_{p,k}^* [\mathbf{X}]_{q,k} \left( \alpha \frac{2\kappa}{N} \sum_p [\mathbf{H}]_{m,p} [\mathbf{H}]_{n,p}^* \right. \\ &\quad \left. + (1 + \beta [\Phi]_{m,m}) \delta_{m-n} \right) \quad (56) \end{aligned}$$

$$\begin{aligned} &= \delta_{p-q} \frac{1}{2T} \left( \alpha \frac{2\kappa}{N} \sum_p [\mathbf{H}]_{m,p} [\mathbf{H}]_{n,p}^* \right. \\ &\quad \left. + (1 + \beta [\Phi]_{m,m}) \delta_{m-n} \right), \quad (57) \end{aligned}$$

where the latter expression follows from the fact that  $\sum_k [\mathbf{X}]_{p,k}^* [\mathbf{X}]_{q,k} = 2T\delta_{p-q}$ , as implied by  $\frac{1}{2T}\mathbf{X}\mathbf{X}^H = \mathbf{I}$ . Equation (57) implies the estimation error is temporally white with  $\mathbf{H}$ -conditional spatial correlation

$$\mathbf{D} \triangleq \frac{1}{2T} \left( \alpha \frac{2\kappa}{N} \mathbf{H}\mathbf{H}^H + \mathbf{I} + \beta \text{diag}(\Phi) \right) \quad (58)$$

$$\begin{aligned} &= \frac{1}{2T} \left( \alpha \frac{2\kappa}{N} \mathbf{H}\mathbf{H}^H + \mathbf{I} \right. \\ &\quad \left. + \beta \left( \alpha \frac{2(1+\kappa)}{N} \text{diag}(\mathbf{H}\mathbf{H}^H) + \mathbf{I} \right) \right). \quad (59) \end{aligned}$$

Our final claim is that the channel estimation error  $\frac{1}{2T}\mathbf{W}\mathbf{X}^H$  is statistically equivalent to  $\mathbf{D}^{\frac{1}{2}}\tilde{\mathbf{H}}$ , with  $\tilde{\mathbf{H}} \in \mathbb{C}^{M \times N}$  constructed from i.i.d  $\mathcal{CN}(0, 1)$  entries. This can be seen from the following:

$$\begin{aligned} & \mathbb{E} \left\{ [\mathbf{D}^{\frac{1}{2}}\tilde{\mathbf{H}}]_{m,p} [\mathbf{D}^{\frac{1}{2}}\tilde{\mathbf{H}}]_{n,q}^* \right\} \\ &= \mathbb{E} \left\{ \sum_k [\mathbf{D}^{\frac{1}{2}}]_{m,k} [\tilde{\mathbf{H}}]_{k,p} \sum_l [\mathbf{D}^{\frac{1}{2}}]_{n,l}^* [\tilde{\mathbf{H}}]_{l,q}^* \right\} \quad (60) \end{aligned}$$

$$= \sum_{k,l} [\mathbf{D}^{\frac{1}{2}}]_{m,k} [\mathbf{D}^{\frac{1}{2}}]_{n,l}^* \mathbb{E} \{ [\tilde{\mathbf{H}}]_{k,p} [\tilde{\mathbf{H}}]_{l,q}^* \} \quad (61)$$

$$= \delta_{p-q} \sum_k [\mathbf{D}^{\frac{1}{2}}]_{m,k} [\mathbf{D}^{\frac{1}{2}}]_{n,k}^* \quad (62)$$

$$= \delta_{p-q} [\mathbf{D}]_{m,n}, \quad (63)$$

where we used the fact that  $\mathbb{E} \{ [\tilde{\mathbf{H}}]_{k,p} [\tilde{\mathbf{H}}]_{l,q}^* \} = \delta_{k-l} \delta_{p-q}$ .

## APPENDIX B INTERFERENCE CANCELLATION DETAILS

In this appendix, we characterize the channel-estimate-conditioned covariance of the aggregate interference  $\mathbf{v}_r$ , whose expression was given in (11).

Recalling that  $\hat{\mathbf{D}} \triangleq \mathbb{E} \{ \mathbf{D} \mid \hat{\mathbf{H}} \}$ , we first establish that  $\text{Cov} \{ \mathbf{D}^{\frac{1}{2}} \tilde{\mathbf{H}} \mathbf{x} \mid \hat{\mathbf{H}} \} = \hat{\mathbf{D}} \text{tr}(\text{Cov}(\mathbf{x}))$ , which will be useful in the sequel. To show this, we examine the  $(m, n)^{th}$  element of

the covariance matrix:

$$[\text{Cov}\{D^{\frac{1}{2}}\tilde{H}\mathbf{x} \mid \hat{H}\}]_{m,n} = \text{E}\{[D^{\frac{1}{2}}\tilde{H}\mathbf{x}]_m [D^{\frac{1}{2}}\tilde{H}\mathbf{x}]_n^* \mid \hat{H}\} \quad (64)$$

$$= \text{E}\left\{\sum_{p,r}[D^{\frac{1}{2}}]_{m,p}[\tilde{H}]_{p,r}[\mathbf{x}]_r \sum_{q,t}[D^{\frac{1}{2}}]_{n,q}^*[\tilde{H}]_{q,t}^*[\mathbf{x}]_t^* \mid \hat{H}\right\} \\ = \sum_{p,r,q,t} \text{E}\{[D^{\frac{1}{2}}]_{m,p}[\tilde{H}]_{p,r}^* \mid \hat{H}\} \\ \times \underbrace{\text{E}\{[\tilde{H}]_{p,r}[\tilde{H}]_{q,t}^*\}}_{\delta_{p-q}\delta_{r-t}} \text{E}\{[\mathbf{x}]_r[\mathbf{x}]_t^*\} \quad (65)$$

$$= [\hat{D}]_{m,n} \text{tr}(\text{Cov}\{\mathbf{x}\}). \quad (66)$$

Rewriting the previous equality in matrix form, we get the desired result. As a corollary, we note that  $\text{E}\{(D^{\frac{1}{2}}\tilde{H})\text{Cov}\{\mathbf{x}\}(D^{\frac{1}{2}}\tilde{H})^H \mid \hat{H}\} = \hat{D} \text{tr}(\text{Cov}\{\mathbf{x}\})$ , which will also be useful in the sequel.

Next we characterize the  $(\hat{H}_{\text{sr}}, \hat{H}_{\text{rr}})$ -conditional covariance of the receiver distortion  $\mathbf{e}_r$ . Recalling that  $\text{Cov}\{\mathbf{e}_r\} = \beta \text{diag}(\Phi_r)$  where  $\Phi_r = \text{Cov}\{\mathbf{u}_r\}$ , we have  $\text{Cov}\{\mathbf{e}_r \mid \hat{H}_{\text{sr}}, \hat{H}_{\text{rr}}\} = \beta \text{diag}(\hat{\Phi}_r)$  where  $\hat{\Phi}_r \triangleq \text{Cov}\{\mathbf{u}_r \mid \hat{H}_{\text{sr}}, \hat{H}_{\text{rr}}\}$ . Then, given that  $\mathbf{u}_r = \mathbf{y}_r - \mathbf{e}_r$  with  $\mathbf{y}_r$  from (10), and using the facts that  $\text{Cov}(\mathbf{x}_s + \mathbf{c}_s) = \mathbf{Q}_s + \kappa \text{diag}(\mathbf{Q}_s)$  and  $\text{Cov}(\mathbf{x}_r + \mathbf{c}_r) = \mathbf{Q}_r + \kappa \text{diag}(\mathbf{Q}_r)$ , we get

$$\hat{\Phi}_r = \rho_r \hat{H}_{\text{sr}}(\mathbf{Q}_s + \kappa \text{diag}(\mathbf{Q}_s))\hat{H}_{\text{sr}}^H \\ + \text{E}\{(D_{\text{sr}}^{\frac{1}{2}}\tilde{H}_{\text{sr}})(\mathbf{Q}_s + \kappa \text{diag}(\mathbf{Q}_s))(D_{\text{sr}}^{\frac{1}{2}}\tilde{H}_{\text{sr}})^H \mid \hat{H}_{\text{sr}}\} \\ + \eta_r \hat{H}_{\text{rr}}(\mathbf{Q}_r + \kappa \text{diag}(\mathbf{Q}_r))\hat{H}_{\text{rr}}^H \\ + \text{E}\{(D_{\text{rr}}^{\frac{1}{2}}\tilde{H}_{\text{rr}})(\mathbf{Q}_r + \kappa \text{diag}(\mathbf{Q}_r))(D_{\text{rr}}^{\frac{1}{2}}\tilde{H}_{\text{rr}})^H \mid \hat{H}_{\text{rr}}\} \\ + \mathbf{I} \quad (67)$$

$$= \rho_r \hat{H}_{\text{sr}}(\mathbf{Q}_s + \kappa \text{diag}(\mathbf{Q}_s))\hat{H}_{\text{sr}}^H \\ + \hat{D}_{\text{sr}} \text{tr}(\mathbf{Q}_s + \kappa \text{diag}(\mathbf{Q}_s)) \\ + \eta_r \hat{H}_{\text{rr}}(\mathbf{Q}_r + \kappa \text{diag}(\mathbf{Q}_r))\hat{H}_{\text{rr}}^H \\ + \hat{D}_{\text{rr}} \text{tr}(\mathbf{Q}_r + \kappa \text{diag}(\mathbf{Q}_r)) + \mathbf{I}. \quad (68)$$

Then,

$$\hat{\Phi}_r = \rho_r \hat{H}_{\text{sr}}(\mathbf{Q}_s + \kappa \text{diag}(\mathbf{Q}_s))\hat{H}_{\text{sr}}^H + (1 + \kappa)\hat{D}_{\text{sr}} \text{tr}(\mathbf{Q}_s) \\ + \eta_r \hat{H}_{\text{rr}}(\mathbf{Q}_r + \kappa \text{diag}(\mathbf{Q}_r))\hat{H}_{\text{rr}}^H \\ + (1 + \kappa)\hat{D}_{\text{rr}} \text{tr}(\mathbf{Q}_r) + \mathbf{I} \quad (69)$$

$$\approx \rho_r \hat{H}_{\text{sr}}\mathbf{Q}_s\hat{H}_{\text{sr}}^H + \hat{D}_{\text{sr}} \text{tr}(\mathbf{Q}_s) \\ + \eta_r \hat{H}_{\text{rr}}\mathbf{Q}_r\hat{H}_{\text{rr}}^H + \hat{D}_{\text{rr}} \text{tr}(\mathbf{Q}_r) + \mathbf{I}, \quad (70)$$

where, for the approximation, we assumed  $\kappa \ll 1$ . Thus,

$$\text{Cov}\{\mathbf{e}_r \mid \hat{H}_{\text{sr}}, \hat{H}_{\text{rr}}\} \\ \approx \beta(\rho_r \text{diag}(\hat{H}_{\text{sr}}\mathbf{Q}_s\hat{H}_{\text{sr}}^H) + \hat{D}_{\text{sr}} \text{tr}(\mathbf{Q}_s) \\ + \eta_r \text{diag}(\hat{H}_{\text{rr}}\mathbf{Q}_r\hat{H}_{\text{rr}}^H) + \hat{D}_{\text{rr}} \text{tr}(\mathbf{Q}_r) + \mathbf{I}). \quad (71)$$

Finally we are ready to characterize  $\hat{\Sigma}_r$ , the  $(\hat{H}_{\text{sr}}, \hat{H}_{\text{rr}})$ -conditional covariance of  $\mathbf{v}_r$ . From (11),

$$\hat{\Sigma}_r = \kappa\rho_r \text{E}\{\mathbf{H}_{\text{sr}} \text{diag}(\mathbf{Q}_s)\mathbf{H}_{\text{sr}}^H \mid \hat{H}_{\text{sr}}\} + \hat{D}_{\text{sr}} \text{tr}(\mathbf{Q}_s) \\ + \kappa\eta_r \text{E}\{\mathbf{H}_{\text{rr}} \text{diag}(\mathbf{Q}_r)\mathbf{H}_{\text{rr}}^H \mid \hat{H}_{\text{rr}}\} + \hat{D}_{\text{rr}} \text{tr}(\mathbf{Q}_r) \\ + \mathbf{I} + \text{Cov}\{\mathbf{e}_r \mid \hat{H}_{\text{sr}}, \hat{H}_{\text{rr}}\} \quad (72)$$

$$= \kappa\rho_r \hat{H}_{\text{sr}} \text{diag}(\mathbf{Q}_s)\hat{H}_{\text{sr}}^H + \mathbf{I} + \text{Cov}\{\mathbf{e}_s \mid \hat{H}_{\text{sr}}, \hat{H}_{\text{rr}}\} \\ + \kappa \text{E}\{(D_{\text{sr}}^{\frac{1}{2}}\tilde{H}_{\text{sr}}) \text{diag}(\mathbf{Q}_s)(D_{\text{sr}}^{\frac{1}{2}}\tilde{H}_{\text{sr}})^H \mid \hat{H}_{\text{sr}}\} \\ + \hat{D}_{\text{sr}} \text{tr}(\mathbf{Q}_s) + \hat{D}_{\text{rr}} \text{tr}(\mathbf{Q}_r) + \kappa\eta_r \hat{H}_{\text{rr}} \text{diag}(\mathbf{Q}_r)\hat{H}_{\text{rr}}^H \\ + \kappa \text{E}\{(D_{\text{rr}}^{\frac{1}{2}}\tilde{H}_{\text{rr}}) \text{diag}(\mathbf{Q}_r)(D_{\text{rr}}^{\frac{1}{2}}\tilde{H}_{\text{rr}})^H \mid \hat{H}_{\text{rr}}\} \quad (73)$$

$$= \kappa\rho_r \hat{H}_{\text{sr}} \text{diag}(\mathbf{Q}_s)\hat{H}_{\text{sr}}^H + (1 + \kappa)\hat{D}_{\text{sr}} \text{tr}(\mathbf{Q}_s) \\ + \kappa\eta_r \hat{H}_{\text{rr}} \text{diag}(\mathbf{Q}_r)\hat{H}_{\text{rr}}^H + (1 + \kappa)\hat{D}_{\text{rr}} \text{tr}(\mathbf{Q}_r) \\ + \mathbf{I} + \text{Cov}\{\mathbf{e}_s \mid \hat{H}_{\text{sr}}, \hat{H}_{\text{rr}}\} \quad (74)$$

$$\approx \mathbf{I} + \kappa\rho_r \hat{H}_{\text{sr}} \text{diag}(\mathbf{Q}_s)\hat{H}_{\text{sr}}^H + \hat{D}_{\text{sr}} \text{tr}(\mathbf{Q}_s) \\ + \kappa\eta_r \hat{H}_{\text{rr}} \text{diag}(\mathbf{Q}_r)\hat{H}_{\text{rr}}^H + \hat{D}_{\text{rr}} \text{tr}(\mathbf{Q}_r) \\ + \beta\rho_r \text{diag}(\hat{H}_{\text{sr}}\mathbf{Q}_s\hat{H}_{\text{sr}}^H) + \beta\eta_r \text{diag}(\hat{H}_{\text{rr}}\mathbf{Q}_r\hat{H}_{\text{rr}}^H), \quad (75)$$

where, for the approximation, we assumed  $\kappa \ll 1$  and  $\beta \ll 1$ , and we leveraged (71).

## APPENDIX C GRADIENT DETAILS

In this appendix, we derive an expression for the gradient  $\nabla_{\mathbf{Q}_r[l]} \underline{I}(\mathbf{Q}, \zeta)$  by first deriving an expression for the derivative  $\frac{\partial \underline{I}}{\partial \mathbf{Q}_r[l]}$  and then using the fact that  $\nabla_{\mathbf{Q}_r[l]} \underline{I} = 2(\frac{\partial \underline{I}}{\partial \mathbf{Q}_r[l]})^*$ .

To do this, we first consider the related problem of computing the derivative  $\partial \det(\mathbf{Y})/\partial \mathbf{X}$ , where

$$\mathbf{Y} \triangleq \mathbf{C} \text{diag}(\mathbf{X})\mathbf{D} + \text{diag}(\mathbf{E}\mathbf{X}\mathbf{F}) + \mathbf{G} \text{tr}(\mathbf{X}) + \mathbf{Z}, \quad (76)$$

and where (76) can be written elementwise as

$$[\mathbf{Y}]_{i,j} = \sum_{m,n} [\mathbf{C}]_{i,m}[\mathbf{X}]_{m,n}[\mathbf{D}]_{n,j}\delta_{m-n} + [\mathbf{Z}]_{i,j} \\ + \sum_{p,q} [\mathbf{E}]_{i,p}[\mathbf{X}]_{p,q}[\mathbf{F}]_{q,j}\delta_{i-j} + [\mathbf{G}]_{i,j} \sum_t [\mathbf{X}]_{t,t}. \quad (77)$$

Notice that, for  $\mathbf{V}_{r,s}$  defined as a zero-valued matrix except for a unity element at row  $r$  and column  $s$ , we have

$$\frac{\partial \det(\mathbf{Y})}{\partial \mathbf{X}} = \sum_{r,s} \mathbf{V}_{r,s} \frac{\partial \det(\mathbf{Y})}{\partial [\mathbf{X}]_{r,s}} \quad (78)$$

$$= \sum_{r,s} \mathbf{V}_{r,s} \sum_{i,j} \frac{\partial \det(\mathbf{Y})}{\partial [\mathbf{Y}]_{i,j}} \frac{\partial [\mathbf{Y}]_{i,j}}{\partial [\mathbf{X}]_{r,s}}. \quad (79)$$

$$\begin{aligned} & \frac{\partial}{\partial \mathbf{Q}_r[l]} \mathcal{I}(\mathbf{Q}_s[1], \mathbf{Q}_s[2], \mathbf{Q}_r[1], \mathbf{Q}_r[2], \zeta) \\ &= \frac{\partial}{\partial \mathbf{Q}_r[l]} \tau[l] \left\{ (1 - \zeta) (\log \det(\mathbf{S}_d[l]) - \log \det(\hat{\mathbf{\Sigma}}_d[l])) + \zeta (\log \det(\mathbf{S}_r[l]) - \log \det(\hat{\mathbf{\Sigma}}_r[l])) \right\} \end{aligned} \quad (83)$$

$$\begin{aligned} &= \frac{\partial}{\partial \mathbf{Q}_r[l]} \tau[l] \left\{ (1 - \zeta) \log \det \left( \rho_d \hat{\mathbf{H}}_{rd} \mathbf{Q}_r[l] \hat{\mathbf{H}}_{rd}^H + \kappa \rho_d \hat{\mathbf{H}}_{rd} \text{diag}(\mathbf{Q}_r[l]) \hat{\mathbf{H}}_{rd}^H + \beta \rho_d \text{diag}(\hat{\mathbf{H}}_{rd} \mathbf{Q}_r[l] \hat{\mathbf{H}}_{rd}^H) + \hat{\mathbf{D}}_{rd} \text{tr} \mathbf{Q}_r[l] + \mathbf{Z}_1[l] \right) \right. \\ &\quad - (1 - \zeta) \log \det \left( \kappa \rho_d \hat{\mathbf{H}}_{rd} \text{diag}(\mathbf{Q}_r[l]) \hat{\mathbf{H}}_{rd}^H + \beta \rho_d \text{diag}(\hat{\mathbf{H}}_{rd} \mathbf{Q}_r[l] \hat{\mathbf{H}}_{rd}^H) + \hat{\mathbf{D}}_{rd} \text{tr} \mathbf{Q}_r[l] + \mathbf{Z}_2[l] \right) \\ &\quad + \zeta \log \det \left( \beta \eta_r \text{diag}(\hat{\mathbf{H}}_{rd} \mathbf{Q}_r[l] \hat{\mathbf{H}}_{rd}^H) + \kappa \eta_r \hat{\mathbf{H}}_{rr} \text{diag}(\mathbf{Q}_r[l]) \hat{\mathbf{H}}_{rr}^H + \hat{\mathbf{D}}_{rr} \text{tr} \mathbf{Q}_r[l] + \mathbf{Z}_3[l] \right) \\ &\quad \left. - \zeta \log \det \left( \beta \eta_r \text{diag}(\hat{\mathbf{H}}_{rd} \mathbf{Q}_r[l] \hat{\mathbf{H}}_{rd}^H) + \kappa \eta_r \hat{\mathbf{H}}_{rr} \text{diag}(\mathbf{Q}_r[l]) \hat{\mathbf{H}}_{rr}^H + \hat{\mathbf{D}}_{rr} \text{tr} \mathbf{Q}_r[l] + \mathbf{Z}_4[l] \right) \right\} \end{aligned} \quad (84)$$

$$\begin{aligned} &= \frac{(1 - \zeta) \rho_d}{\ln 2} \tau[l] \left\{ (\hat{\mathbf{H}}_{rd}^H [\mathbf{S}_d^{-1}[l] + \beta \text{diag}(\mathbf{S}_d^{-1}[l] - \hat{\mathbf{\Sigma}}_d^{-1}[l])] \hat{\mathbf{H}}_{rd})^T + \kappa \text{diag}(\hat{\mathbf{H}}_{rd}^H (\mathbf{S}_d^{-1}[l] - \hat{\mathbf{\Sigma}}_d^{-1}[l]) \hat{\mathbf{H}}_{rd}) \right\} \\ &\quad + \frac{1 - \zeta}{\ln 2} \tau[l] \text{sum}(\hat{\mathbf{D}}_{rd} \odot (\mathbf{S}_d^{-1}[l] - \hat{\mathbf{\Sigma}}_d^{-1}[l])^T) \mathbf{I} + \frac{\zeta \eta_r}{\ln 2} \tau[l] \left\{ \kappa \text{diag}(\hat{\mathbf{H}}_{rr}^H (\mathbf{S}_r^{-1}[l] - \hat{\mathbf{\Sigma}}_r^{-1}[l]) \hat{\mathbf{H}}_{rr}) \right. \\ &\quad \left. + \beta (\hat{\mathbf{H}}_{rd}^H \text{diag}(\mathbf{S}_r^{-1}[l] - \hat{\mathbf{\Sigma}}_r^{-1}[l]) \hat{\mathbf{H}}_{rd})^T \right\} + \frac{\zeta}{\ln 2} \tau[l] \text{sum}(\hat{\mathbf{D}}_{rr} \odot (\mathbf{S}_r^{-1}[l] - \hat{\mathbf{\Sigma}}_r^{-1}[l])^T) \mathbf{I}. \end{aligned} \quad (85)$$

Then, using (77), we get

$$\begin{aligned} & \frac{\partial \det(\mathbf{Y})}{\partial \mathbf{X}} \\ &= \sum_{r,s} \mathbf{V}_{r,s} \sum_{i,j} \frac{\partial \det(\mathbf{Y})}{\partial [\mathbf{Y}]_{i,j}} \left( [\mathbf{C}]_{i,r} [\mathbf{D}]_{s,j} \delta_{r-s} \right. \\ &\quad \left. + [\mathbf{E}]_{i,r} [\mathbf{F}]_{s,j} \delta_{i-j} + [\mathbf{G}]_{i,j} \delta_{r-s} \right) \end{aligned} \quad (80)$$

$$\begin{aligned} &= \text{diag} \left( \mathbf{D} \left( \frac{\partial \det \mathbf{Y}}{\partial \mathbf{Y}} \right)^T \mathbf{C} \right) + \left( \mathbf{F} \text{diag} \left( \frac{\partial \det \mathbf{Y}}{\partial \mathbf{Y}} \right)^T \mathbf{E} \right)^T \\ &\quad + \text{sum} \left( \mathbf{G} \odot \left( \frac{\partial \det \mathbf{Y}}{\partial \mathbf{Y}} \right) \right) \mathbf{I} \end{aligned} \quad (81)$$

$$\begin{aligned} &= \det(\mathbf{Y}) \left( \text{diag}(\mathbf{D} \mathbf{Y}^{-1} \mathbf{C}) + (\mathbf{F} \text{diag}(\mathbf{Y}^{-1}) \mathbf{E})^T \right. \\ &\quad \left. + \text{sum}(\mathbf{G} \odot (\mathbf{Y}^{-1})^T) \mathbf{I} \right), \end{aligned} \quad (82)$$

where, for the last step, we used the fact that  $\frac{\partial \det(\mathbf{Y})}{\partial \mathbf{Y}} = \det(\mathbf{Y}) (\mathbf{Y}^{-1})^T$ .

Applying (82) to (22), we can obtain an expression for  $\frac{\partial \mathcal{I}}{\partial \mathbf{Q}_r[l]}$ . To do so, we think of  $\mathbf{Z}$  in (76) as representing the terms in  $\mathcal{I}$  that have zero derivative with respect to  $\mathbf{Q}_r[l]$ . Using  $\mathbf{S}_d[l]$  and  $\mathbf{S}_r[l]$  defined in (37)-(38), and recalling the expression for  $\hat{\mathbf{\Sigma}}_d[l]$  in (13), the result is given in (85), at the top of the page.

Finally, using  $\mathbf{G}_r[l] = 2 \left( \frac{\partial \mathcal{I}}{\partial \mathbf{Q}_r[l]} \right)^*$ , and leveraging the fact that  $\mathbf{S}_d[l]$ ,  $\mathbf{S}_r[l]$ ,  $\hat{\mathbf{\Sigma}}_d[l]$ , and  $\hat{\mathbf{\Sigma}}_r[l]$  are Hermitian matrices, we get the expression for  $\mathbf{G}_r[l]$  in (36). A similar expression results for  $\mathbf{G}_s[l]$ .

## REFERENCES

- [1] M. Jain, J. I. Choi, T. M. Kim, D. Bharadia, S. Seth, K. Srinivasan, P. Levis, S. Katti, and P. Sinha, "Practical, real-time, full duplex wireless," in *Proc. ACM Internat. Conf. Mobile Comput. & Netw.*, (Las Vegas, NV), pp. 301–312, Sept. 2011.
- [2] E. Everett, M. Duarte, C. Dick, and A. Sabharwal, "Empowering full-duplex wireless communication by exploiting directional diversity," in *Proc. Asilomar Conf. Signals Syst. Comput.*, pp. 2002–2006, Nov. 2011.
- [3] Y. Hua, "An overview of beamforming and power allocation for MIMO relays," in *Proc. IEEE Military Commun. Conf.*, (San Jose, CA), pp. 375–380, Nov. 2010.
- [4] B. Wang, J. Zhang, and A. Høst-Madsen, "On the capacity of MIMO relay channels," *IEEE Trans. Inform. Theory*, vol. 51, pp. 29–43, Jan. 2005.
- [5] S. Simoens, O. Muñoz-Medina, J. Vidal, and A. del Coso, "On the Gaussian MIMO relay channel with full channel state information," *IEEE Trans. Signal Process.*, vol. 57, pp. 3588–3599, Sep. 2009.
- [6] D. W. Bliss, P. A. Parker, and A. R. Margetts, "Simultaneous transmission and reception for improved wireless network performance," in *Proc. IEEE Workshop Statist. Signal Process.*, (Madison, WI), pp. 478–482, Aug. 2007.
- [7] P. Larsson and M. Prytz, "MIMO on-frequency repeater with self-interference cancellation and mitigation," in *Proc. IEEE Veh. Tech. Conf.*, (Barcelona, Spain), pp. 1–5, Apr. 2009.
- [8] T. Riihonen, S. Werner, and R. Wichman, "Spatial loop interference suppression in full-duplex MIMO relays," in *Proc. Asilomar Conf. Signals Syst. Comput.*, (Pacific Grove, CA), pp. 1508–1512, Nov. 2009.
- [9] T. Riihonen, S. Werner, and R. Wichman, "Residual self-interference in full-duplex MIMO relays after null-space projection and cancellation," in *Proc. Asilomar Conf. Signals Syst. Comput.*, (Pacific Grove, CA), pp. 653–657, Nov. 2010.
- [10] T. Riihonen, A. Balakrishnan, K. Haneda, S. Wyne, S. Werner, and R. Wichman, "Optimal eigenbeamforming for suppressing self-interference in full-duplex MIMO relays," in *Proc. Conf. Inform. Science & Syst.*, (Baltimore, MD), pp. 1–5, Mar. 2011.
- [11] S. Sohaib and Daniel K.C. So, "Asynchronous polarized cooperative MIMO communication," in *Proc. IEEE Veh. Tech. Conf.*, (Barcelona, Spain), pp. 1–5, Apr. 2009.
- [12] J. Sangiamwong, T. Asai, J. Hagiwara, Y. Okumura, and T. Ohya, "Joint multi-filter design for full-duplex MU-MIMO relaying," in *Proc. IEEE Veh. Tech. Conf.*, (Barcelona, Spain), pp. 1–5, Apr. 2009.
- [13] B. Chun, E.-R. Jeong, J. Joung, Y. Oh, and Y. H. Lee, "Pre-nulling for self-interference suppression in full-duplex relays," in *Proc. APSIPA Annual Summit and Conf.*, (Sapporo, Japan), pp. 91–97, Oct. 2009.
- [14] B. Chun and Y. H. Lee, "A spatial self-interference nullification method for full duplex amplify-and-forward MIMO relays," in *Proc. IEEE Wireless Commun. & Netw. Conf.*, (Sydney, Australia), pp. 1–6, Apr. 2010.
- [15] P. Lioliou, M. Viberg, M. Coldrey, and F. Athley, "Self-interference suppression in full-duplex MIMO relays," in *Proc. Asilomar Conf. Signals Syst. Comput.*, (Pacific Grove, CA), pp. 658–662, Oct. 2010.
- [16] G. Santella and F. Mazzenga, "A hybrid analytical-simulation procedure for performance evaluation in M-QAM-OFDM schemes in presence of



nonlinear distortions," *IEEE Trans. Veh. Tech.*, vol. 47, pp. 142–151, Feb. 1998.

- [17] H. Suzuki, T. V. A. Tran, I. B. Collings, G. Daniels, and M. Hedley, "Transmitter noise effect on the performance of a MIMO-OFDM hardware implementation achieving improved coverage," *IEEE J. Sel. Areas Commun.*, vol. 26, pp. 867–876, Aug. 2008.
- [18] R. M. Gray and T. G. Stockham, Jr., "Dithered quantizers," *IEEE Trans. Inform. Theory*, vol. 39, pp. 805–812, May 1993.
- [19] W. Namgoong, "Modeling and analysis of nonlinearities and mismatches in AC-coupled direct-conversion receiver," *IEEE Trans. Wireless Commun.*, vol. 4, pp. 163–173, Jan. 2005.
- [20] B. Hassibi and B. M. Hochwald, "How much training is needed in multiple-antenna wireless links," *IEEE Trans. Inform. Theory*, vol. 49, pp. 951–963, Apr. 2003.
- [21] D. Tse and P. Viswanath, *Fundamentals of Wireless Communication*. New York: Cambridge University Press, 2005.
- [22] D. Bertsekas, *Nonlinear Programming*. Athena Scientific, 2nd ed., 1999.
- [23] Y. Rong and Y. Hua, "Optimal power schedule for distributed MIMO links," *IEEE Trans. Wireless Commun.*, vol. 7, pp. 2896–2900, Aug. 2008.



**Brian P. Day** received the B.S. in Electrical and Computer Engineering from The Ohio State University in 2010. Since 2010, he has been working toward the Ph.D degree in Electrical and Computer Engineering at The Ohio State University. His primary research interests are full-duplex communication, signal processing, and optimization.



**Adam R. Margetts** received a dual B.S. degree in Electrical Engineering and Mathematics from Utah State University, Logan, UT in 2000; and the M.S. and Ph.D. degrees in Electrical Engineering from The Ohio State University, Columbus, OH in 2002 and 2005, respectively. Dr. Margetts has been with MIT Lincoln Laboratory, Lexington, MA since 2005 and holds two patents in the area of signal processing for communications. His current research interests include distributed transmit beamforming, cooperative communications, full-duplex relay systems, space-time coding, and wireless networking.



**Daniel W. Bliss** is a senior member of the technical staff at MIT Lincoln Laboratory in the Advanced Sensor Techniques group. Since 1997 he has been employed by MIT Lincoln Laboratory, where he focuses on adaptive signal processing, parameter estimation bounds, and information theoretic performance bounds for multisensor systems. His current research topics include multiple-input multiple-output (MIMO) wireless communications, MIMO radar, cognitive radios, radio network performance bounds, geolocation techniques, channel phenomenology, and signal processing and machine learning for anticipatory medical monitoring.

Dan received his Ph.D. and M.S. in Physics from the University of California at San Diego (1997 and 1995), and his BSEE in Electrical Engineering from Arizona State University (1989). Employed by General Dynamics (1989–1991), he designed avionics for the Atlas-Centaur launch vehicle, and performed research and development of fault-tolerant avionics. As a member of the superconducting magnet group at General Dynamics (1991–1993), he performed magnetic field calculations and optimization for high-energy particle-accelerator superconducting magnets. His doctoral work (1993–1997) was in the area of high-energy particle physics, searching for bound states of gluons, studying the two-photon production of hadronic final states, and investigating innovative techniques for lattice-gauge-theory calculations.



**Philip Schniter** received the B.S. and M.S. degrees in Electrical and Computer Engineering from the University of Illinois at Urbana-Champaign in 1992 and 1993, respectively. From 1993 to 1996 he was employed by Tektronix Inc. in Beaverton, OR as a systems engineer, and in 2000, he received the Ph.D. degree in Electrical Engineering from Cornell University in Ithaca, NY. Subsequently, he joined the Department of Electrical and Computer Engineering at The Ohio State University in Columbus, OH, where he is now an Associate Professor and a member of the Information Processing Systems (IPS) Lab. In 2003, he received the National Science Foundation CAREER Award, and in 2008–2009 he was a visiting professor at Eurecom (Sophia Antipolis, France) and Supélec (Gif-sur-Yvette, France). Dr. Schniter's areas of interest include statistical signal processing, wireless communications and networks, and machine learning.